

Whole-rock and mineral chemistry characterization of contrasting granitoids, constraints on the source of the Vieirópolis NYF-type pegmatites, Northeastern Brazil

Igor Manoel Belo de Albuquerque e Souza^{1*} , Ignez de Pinho Guimarães¹ ,
Sandra de Brito Barreto¹ , Glenda Lira Santos¹ , José Ferreira de Araújo Neto¹ 

Abstract

The Vieirópolis pegmatite field is characterized by amazonite pegmatites inserted in the Borborema Province. The Serra Branca pegmatite is hosted by the Serra Branca granites, which intruded partially the Serra Negra granites, and stands out by its amazonite mineralization. To comprehend the crystallization conditions and the source of this pegmatite and associated Serra Branca and Serra Negra granites, petrographic, mineral chemistry, geochronological and whole-rock geochemical data were used. The Serra Branca pegmatite is Cs-, Rb-, Pb-, Nb-, and Ta-rich. The Serra Branca granites (563 ± 2 Ma) are metaluminous to weakly peraluminous, crystallized under high fO_2 conditions, pressure of 2.68–2.80 kbar and temperatures ranging from 667–670°C, with many zircon grains showing inherited cores of Paleoproterozoic ages. The Serra Negra granites (594 ± 4 Ma) comprises metaluminous granites crystallized under high fO_2 conditions, temperatures within 711–751°C, pressure varying from 4.72 to 5.42 kbar. Both granites resulted from distinct partial melting degrees of a source similar to the Caicó Complex orthogneisses. The Serra Branca pegmatite geochemical data suggests that it was originated by extreme fractionation of the Serra Branca granites magma. The Serra Branca amazonite pegmatite is the first pegmatite mineralogically and geochemically characterized as Nb-Y-F (NYF)-type from the gadolinite subtype in the Borborema Province.

KEYWORDS: Serra Branca amazonite pegmatite; NYF-type pegmatite; mineral chemistry; crystallization conditions; whole-rock geochemistry.

INTRODUCTION

The Borborema Province (BP) in Northeastern Brazil hosts one of the largest, in global scale, pegmatite Province — the Seridó Pegmatite Province (SPP; Santos *et al.* 2014), located in the Rio Grande do Norte domain of the Northern sub-province. The pegmatites from the SPP are known since the First World War when the mica exploitation started. By the end of the Second World War, the SPP became globally famous due to the production of Ta ore and the beautiful species of exotic minerals (Beurlen *et al.* 2009). According to Černý (1991a, 1991b) and Černý and Ercit (2005), the SPP pegmatites are classified as belonging to the Li-Ce-Ta (LCT) Family rare elements class, within the beryl-columbite, beryl-columbite-phosphate and spodumene sub-types (Da Silva *et al.* 1995, Beurlen *et al.* 2008). Besides the SPP, the Northern sub-province hosts the Solonópoles-Quixeramobim pegmatite district in the Ceará domain (Souza 1985). The pegmatites in the Solonópoles-Quixeramobim district are dominantly LCT-type, and the

presence of gemstones, industrial minerals and others of economic values (beryl, cassiterite, amblygonite, tantalite, columbite, lepidolite and spodumene) has been reported (Vidal & Nogueira Neto 2005). Many others isolated occurrences of pegmatite are described in the Northern sub-province of the BP (Santos *et al.* 2014).

The Vieirópolis pegmatite field was reported for the first time by Barreto *et al.* (2016), and it constitutes the first reported occurrence of a pegmatite field out of the SPP, in the Rio Grande do Norte domain. The Vieirópolis pegmatite field is characterized by amazonite- and/or beryl-bearing pegmatites. The presence of amazonite classifies these pegmatites as Nb-Y-F (NYF)-type (Martin *et al.* 2008), thus, being the first NYF-type pegmatite identified in the BP.

This paper focuses on the study of two plutons (Serra Branca and Serra Negra) and the Serra Branca amazonite pegmatite of the Vieirópolis field. We present petrographic, U-Pb geochronological data, mineral and whole-rock chemical data to constraint the conditions of magmatic crystallization and the sources of both granites and the pegmatite.

¹Universidade Federal de Pernambuco – Recife (PE), Brazil.
E-mails: igor.manoel.belo@gmail.com, ignez@ufpe.br,
sandradebritobarreto@gmail.com, glendaliraa@gmail.com,
araujoneto.geo@gmail.com

*Corresponding author.



REGIONAL GEOLOGY

The BP (Almeida *et al.* 1981) comprehends an area of ~450,000 km², in Northeastern Brazil, and it is limited to the south by the São Francisco Craton, to the west by the Parnaíba Basin, and to the north and east by coastal basins. The BP

comprises Paleoproterozoic gneiss-migmatitic complexes, small Archean nuclei and Neoproterozoic to Mesoproterozoic supracrustal sequences (Van Schmus *et al.* 1995, 2008, Neves *et al.* 2008, Guimarães *et al.* 2016, Silva Filho *et al.* 2016). According to Van Schmus *et al.* (2008), the province resulted from the breakup of a Paleoproterozoic supercontinent, Atlantica (Rogers 1996), during the late Mesoproterozoic to early Neoproterozoic. This event was associated with volcanism (mostly felsic) and granitic intrusions, deposition of extensional basins floored by Paleoproterozoic crust approaching small oceans, and a larger ocean between the northern edge of Congo-São Francisco and the West African-Sao Luis cratons.

The actual framework of the BP resulted from the Brasiliano (Pan-African) Orogeny (650–550 Ma; Van Schmus *et al.* 2008), which was responsible for extensive granitic magmatism along with large scale transcurrent shear zones, where the granites are commonly used to date the Brasiliano deformations. Such transcurrent shear zones formed contemporaneous conjugate sets of sinistral NE-SW striking and dextral E-W striking mylonitic belts developed under middle- to high temperature amphibolite facies conditions (Vauchez & Egydio-Silva 1992, Guimarães & Da Silva Filho 1998, Ferreira *et al.* 1998, Neves & Mariano 1999, Neves *et al.* 2000, Silva & Mariano 2000, Neves *et al.* 2006).

Van Schmus *et al.* (1995), using the E-W trending Pernambuco and Patos shear zones with dextral kinematics, divided the BP into three major domains, later renamed to sub-provinces (Van Schmus *et al.* 2011; Fig. 1A): Northern, Transversal and Southern. Each sub-province was divided into domains. The Northern sub-province is subdivided into Rio Grande do Norte, Ceará and Médio Coreá domains. The studied area is located within the Rio Grande do Norte domain.

The Rio Grande do Norte domain (RGND) is a Rhyacian to Orosirian crustal block bordered in the south by the Patos shear zone and at the west by the Ceará domain (Van Schmus

et al. 2011). Besides the Paleoproterozoic rocks, which comprise the Serrinha Pedro Velho and Caicó complexes, it also encloses an Archean nucleus (São José do Campestre) and the NE-trending metasedimentary Seridó Fold Belt. In the RGND, the granitic magmatism is associated to large scale shear zones (Jardim de Sá 1994, Van Schmus *et al.* 1995, Dantas 1997, Brito Neves *et al.* 2000, Jardim de Sá *et al.* 1981) and have crystallization ages ranging from 575 to 540 Ma (McMurry *et al.* 1987, Leterrier *et al.* 1994, Jardim de Sá 1994, Trindade *et al.* 1999, Hollanda *et al.* 2003, Guimarães *et al.* 2009, Nascimento *et al.* 2015). Ages younger than 540 Ma (Rb–Sr method) have been recorded by Nascimento *et al.* (2000), in alkaline intrusions within the Paleoproterozoic Serrinha–Pedro Velho Complex, which is part of the São José do Campestre domain.

GEOLOGICAL FRAMEWORK AND PETROGRAPHY OF THE VIEIRÓPOLIS AREA

The studied area comprises a Paleoproterozoic basement (Caicó Complex and Poço da Cruz Suite), granitic intrusions (Serra Negra and Serra Branca granitoids) and pegmatite dykes (Fig. 2). The regional NE-SW trend seen in the basement and granitic bodies is associated with the Vieirópolis and Lastro dextral transcurrent shear zones (Araújo Neto *et al.* 2018). A brittle regime is also characterized by fractures and/or faults predominantly in a NW-SE, and E-W direction is subordinated, cross-cutting the main structures. In regions near to the shear zones, this fracturing pattern is transversal to the mylonitic foliation.

The Caicó Complex (2.25–2.15 Ga) is the high-grade basement of the metasedimentary Seridó Group. It is composed of an older metavolcanosedimentary unit, and a younger and most common metaplutonic unit consisting locally of migmatized

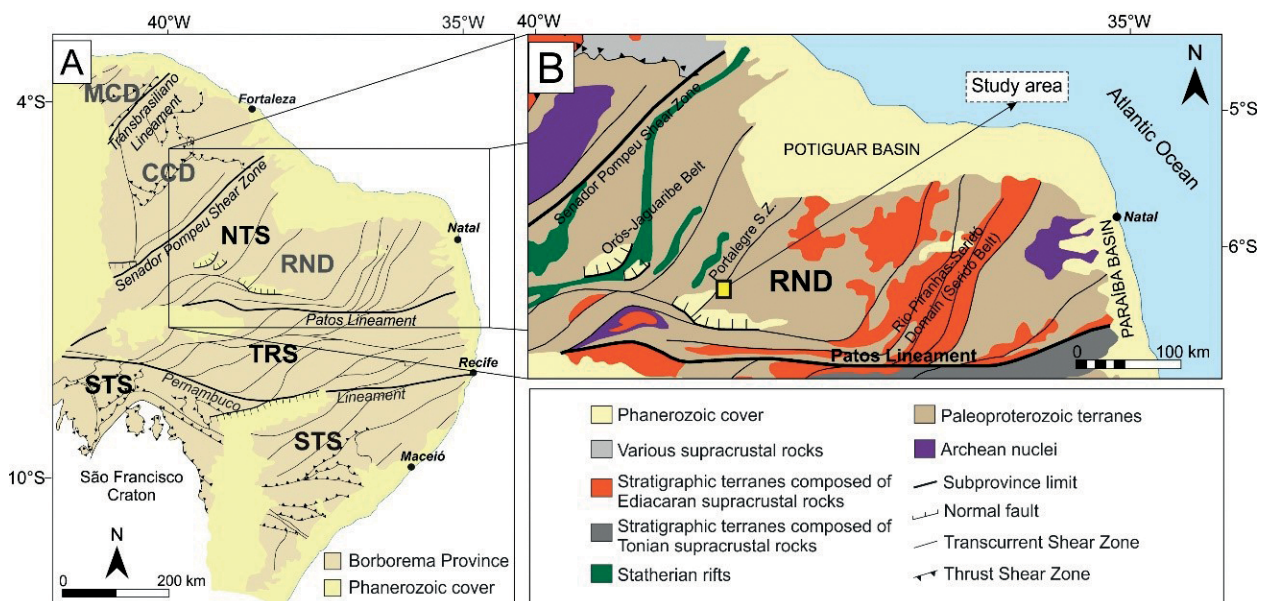


Figure 1. (A) Tectonic Division of the Borborema Province. (B) Schematic geologic map of the Northern sub-province and the location of the studied area. MCD: Médio Coreá domain; CCD: Ceará Central; RND: Rio Grande do Norte domain; NTS: Northern Sub-province; TRS: Sub-province Transversal; STS: Sub-province South. Modified from Santos *et al.* (2014) with subdivisions according to Van Schmus *et al.* (2011).

high-K calc-alkaline orthogneisses, ranging in composition from diorite to granite containing mafic enclaves and elongated amphibolite bodies (Meunier 1964, Ferreira & Albuquerque 1969). According to Souza *et al.* (2007) the Caicó orthogneisses were generated by melting of a metasomatically enriched spinel- to garnet-bearing lherzolite in a subduction zone setting.

The Rhyacian Poço da Cruz Suite ($2,172 \pm 24$ Ma; Hollanda *et al.* 2011, Sá *et al.* 2014) is composed of syenogranitic augen gneisses, with K-feldspars porphyroclasts and lenses of dioritic composition. The studied area comprises a NE-trending elongate body, intruded into the Caicó Complex at the south of the Lastro Shear Zone.

The Serra Negra granitoids is formed by four NE-trending plutons of different sizes, whose emplacement were controlled by the dextral kinematic Lastro and Vieirópolis shear zones (Araújo Neto *et al.* 2018; Fig. 2). These granitoids are medium to coarse-grained, porphyritic, with K-feldspar phenocrysts enclosing quartz and plagioclase crystals, and compositions ranging from quartz monzonite to syenite (Fig. 3A). The plagioclase is presented as subhedral crystals, some of them showing lamellar deformation. Anhedral quartz crystals showed undulatory extinction. Biotite and calcic amphiboles (Fig. 3B) are the principal mafic mineral phases and occur in modal concentrations of 7.0–1.0%, 23–3.5% respectively. Titanite, epidote and magnetite (Fig. 3C) are the main accessory phases. The diorite and porphyritic granite enclaves are angular in shape. Some of them enclose rounded amphibole clots, and some show evidence of partial melting (Fig. 3D).

The Serra Branca pluton is intruded into the NE-trending Serra Negra pluton. Both plutons intrude the Paleoproterozoic orthogneisses and migmatites of the Caicó Complex. The Serra Branca pluton is composed of medium grained monzogranites to quartz monzonites (Fig. 4A) and it is the host rocks of the Vieirópolis pegmatites. Amphibole, pyroxene \pm biotite are the main mafic mineral phases, with modal percentage varying from 10 to 20%. Anhedral quartz crystals showed undulose

extinction. Pyroxene occurs as subhedral to anhedral crystals. Amphibole occurs as subhedral isolated crystals or replacing pyroxene (Fig. 4B). Epidote, allanite, titanite, apatite and opaque minerals constitute the accessory phases. Euhedral to anhedral magnetite crystals makes up the main opaque minerals. Under reflected light, the magnetite shows pinkish gray color with white rims (Fig. 4C). At the contact with the pegmatites, the Serra Branca granites are fine grained, showing higher concentration of mafic minerals and, less frequently, portions of quartz and plagioclase with saccharoidal texture (Fig. 4D). These features may suggest differences in temperature and magmatic fluid percolation during the emplacement of the pegmatite.

U-Pb TIMS zircon ages were reported by Medeiros *et al.* (2005) at 571 ± 3 Ma for granitoids correlated to the Serra Negra granites and at 541 ± 4 Ma to granitoids correlated to the Serra Branca granites.

The pegmatites in the Vieirópolis field comprise four dykes of amazonite-bearing NYF- type pegmatites, hosted by the Serra Branca granite (Fig. 2). Within these pegmatite bodies, the Serra Branca amazonite pegmatite is distinct from other pegmatites of the Vieirópolis pegmatite field and from other well-known pegmatites of the BP by the presence of amazonite megacrysts, which can reach up to 2m of length.

The Serra Branca amazonite pegmatite constitutes an 800 m long, NW- trending dipping 45° to WSW dyke. Two zones were identified:

- the amazonite zone;
- the albite zone.

The amazonite zone commonly occurs at the top of the pegmatite, and the albite zone in the bottom (Fig. 5A). The contacts between the two zones are irregular, complex and usually characterized by the presence of elongated quartz and patches of small biotite crystals. The main mineral phases of the amazonite zone are large amazonite crystals and quartz. The amazonite is prismatic and euhedral to subhedral, varying

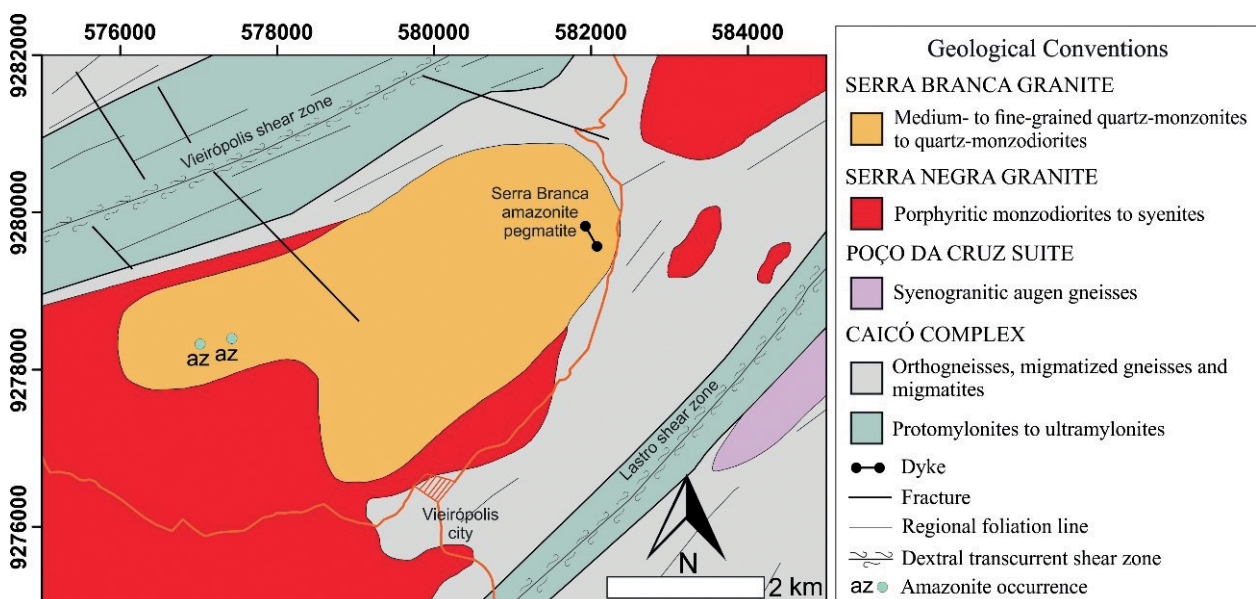


Figure 2. Geologic simplified map of the Vieirópolis pegmatitic field. Modified from Araújo Neto *et al.* (2018).

from centimeter to meter in size and showing bluish green color (Fig. 5B), perthitic exsolution and sometimes graphic texture. The quartz occurs as euhedral to subhedral crystals, with the larger crystals displaying a pseudo-hexagonal habit, with color varying from smoky to colorless (Fig. 5B). The amazonite megacrysts are fractured, and the fractures, as well as the contacts between the amazonite and quartz, are filled up with saccharoidal and/or platy white albite (cleavelandite) and quartz. In this zone, occur a large variety of accessory minerals. Biotite is the most abundant accessory mineral phase appearing as black plates up to 10 cm long, without a preferential direction (Fig. 5C). Sulphides (galena and aikinite) have centimeter to decimeter irregular cluster (Fig. 5D). Chalcocite was recorded as intergrowths in the galena cleavages (Fig. 5E). Small cavities with diameters up to 0.5 cm are commonly filled up with pyromorphite, cerussite, bismutite and anglesite. Another cavity-type with secondary minerals was found in the central part of the amazonitic zone filled with fluorite, muscovite, helvine, phenakite, biotite, ilmenite, pyromorphite, rutile, pyrochlore, montmorillonite and illite. Helvine occurs as centimeter crystals enclosed by amazonite (Fig. 5F). The ilmenite occurs as centimeter anhedral crystals disseminated between the amazonite and quartz megacrystals.

The albite zone is composed mainly of saccharoidal whitish albite, hyaline quartz and less frequent cleavelandite (Fig. 5B).

Rare centimeter fractured amazonite crystals and pseudo hexagonal smoky quartz crystals are recorded in the albite zone. The fractures in the amazonite and quartz crystals are filled with saccharoidal albite and quartz. Biotite, ilmenite, zircon, Mn-columbite, spessartite and pyrochlore minerals make up the accessory phases.

MINERAL CHEMISTRY

Plagioclase, K-feldspar, biotite, amphibole, titanite and opaque minerals were analyzed from 11 samples, using a JEOL JXA-8230 model electronic microprobe equipment, equipped with five WDS and one EDS spectrometers at the Microprobe Laboratory of the Universidade de Brasilia. For major elements analyses, they were used an acceleration voltage of 15V, a current of 10 nA and an electronic bin in the order of μm . For analyses of rare earth elements (REE) in titanite, they were used an acceleration voltage of 20V and a current of 20nA. The used international standards were REE-oxide synthetic glass. The WDS REE corrections followed the Williams (1996) recommendations.

Biotite

Biotite was analyzed from the Serra Branca (45 crystals) and Serra Negra (30 crystals) granitoids and from the

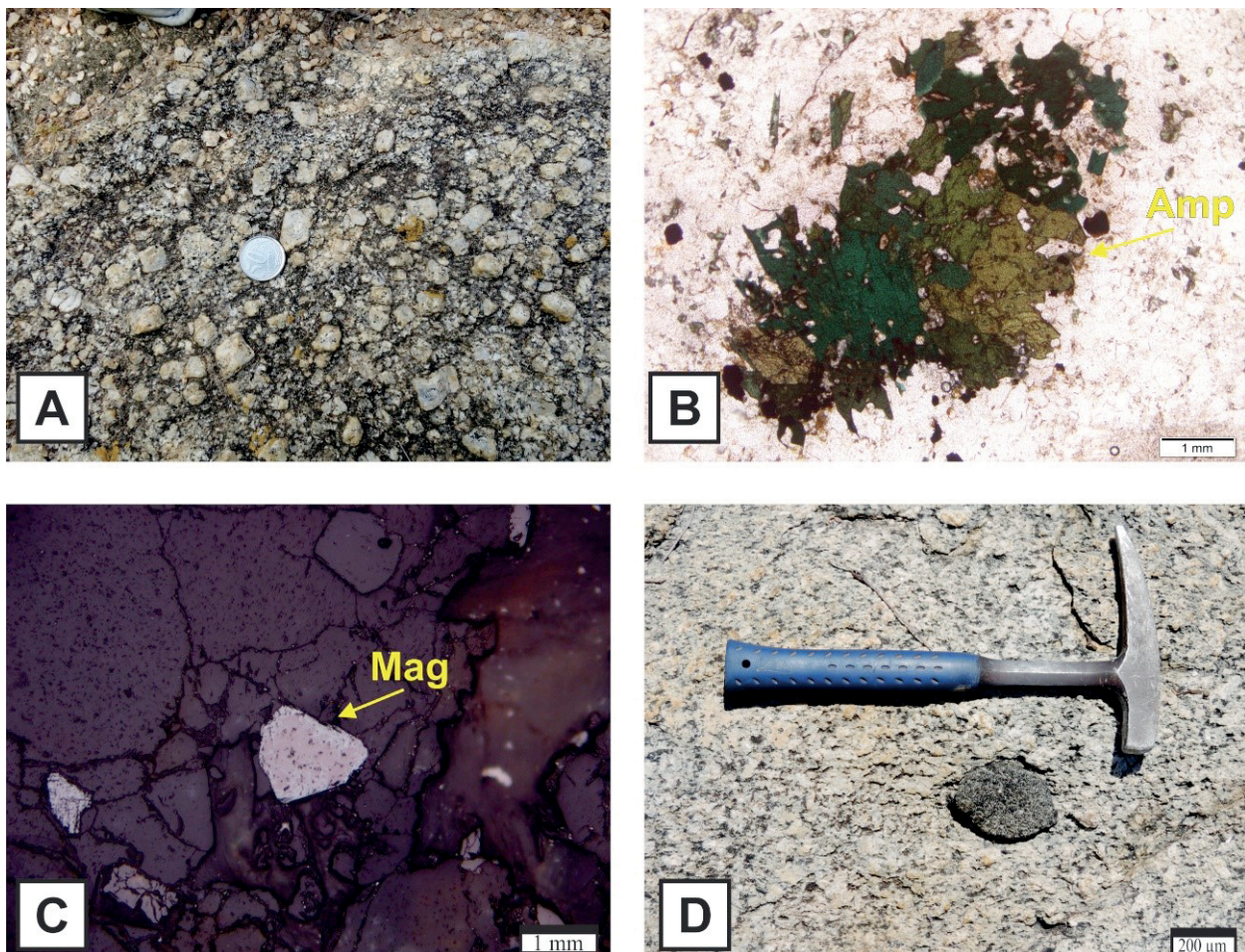


Figure 3. Field and microscopic aspects of the Serra Negra granites; (A) Porphyritic texture with K-feldspar phenocrysts; (B) Clots of amphibole (Amp); (C) Subhedral crystal of magnetite (Mag) under reflected light; (D) Igneous mafic enclaves.

Serra Branca pegmatite (3 crystals), totaling 78 analyses. The results are shown in Table 1. Biotite analyzed from the Serra Negra granites show Fe# $[Fe/(Fe + Mg)]$ values ranging from 0.404 to 0.356, which are like those recorded in biotite from the Serra Branca amazonite pegmatite (Fig. 6A). The biotite from the Serra Branca granitoids shows higher Fe# values (0.591 to 0.499). In the Al^{IV} versus Fe diagram (Fig. 6A), the biotites analyzed from the Serra Branca and Serra Negra granitoids show compositions between annite and phlogopite, while biotite analyzed from the Serra Branca amazonite pegmatite are plotting close to the phlogopite field. In the diagram proposed by Nachit *et al.* (1985), the biotite analyzed from the Serra Negra granitoids plot in the field of those biotites from granitoids of the subalkaline series while the analyzed biotite crystals from the Serra Branca granitoids plot dominantly within the field of biotites from granitoids of alkaline series (Fig. 6B).

Amphibole

Forty-six and forty-seven amphibole crystals were analyzed from the Serra Negra and Serra Branca granitoids, respectively. The results are shown in Table 2. According to Czamanske and Wones (1973), Si versus $(Na + K + Ca)$ discriminates magmatic amphiboles from that tardi- to post magmatic. The amphiboles

analyzed from the Serra Negra and Serra Branca granitoids have composition falling in both fields (Fig. 7A). According to the diagram for amphibole discrimination from Leake *et al.* (1997), the magmatic amphiboles of the Serra Negra granite show composition ranging from ferro-edenite to ferropargasite (Fig. 7B), while the tardi- to post magmatic amphiboles have composition ranging from edenite to Mg-hornblende (Fig. 7C). The magmatic amphiboles from the Serra Branca granites are edenite and tardi to post-magmatic amphiboles are actinolite (Fig. 7B and 7C).

The magmatic amphiboles from both studied granites have low Fe# $(Fe/(Fe + Mg))$ values suggesting crystallization under high fO_2 (Fig. 7D). However, the magmatic amphiboles from the Serra Negra granites have Fe# values (0.424 to 0.663) slight higher than those analyzed from the Serra Branca granites (0.478 a 0.533), reflecting the simultaneous crystallization of biotite and amphibole during the cooling of the Serra Branca granitic magma, and an early crystallization of amphibole in the Serra Negra granitic magmas.

Feldspars

Eighty-eight feldspar grains, including plagioclase (Pl) and K-feldspars (Kfs), were analyzed from the Serra Negra (Kfs = 14 and Pl = 15 crystals) and Serra Branca (Kfs = 7 and

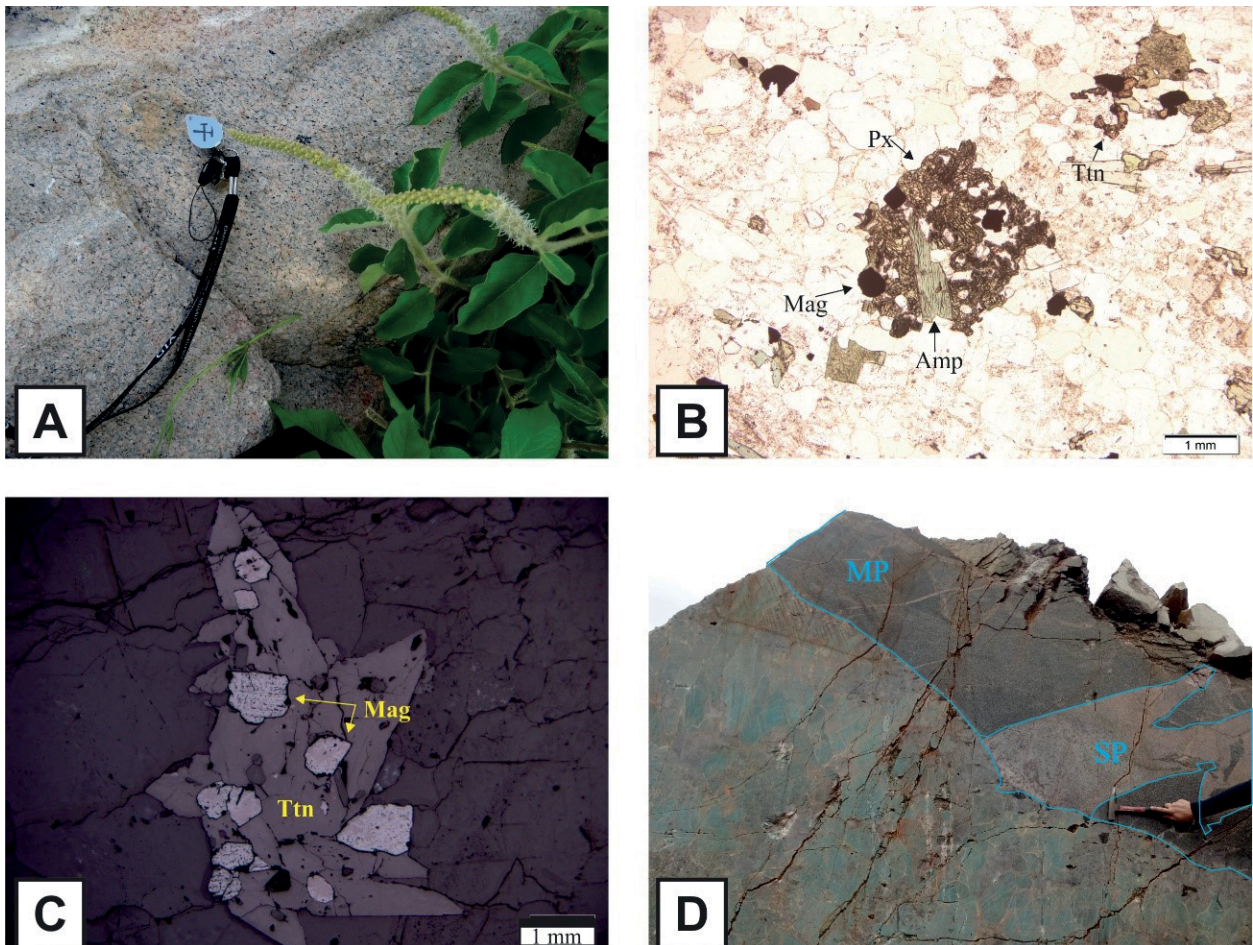


Figure 4. Field and petrographic aspects of the Serra Branca granite: (A) Medium grained Serra Branca granite *in situ* exhibiting greyish color; (B) lot of amphibole (Amp) and magnetite (Mag) replacing pyroxene (Px); (C) Magnetite crystals (Mag) included by titanite (Tit) under reflected light; (D) The contact between the Serra Branca granite and the Serra Branca amazonite pegmatite showing concentration of mafics along the contact (MP) and portion of saccharoidal texture (SP).

Pl = 29 crystals) granites and Serra Branca amazonite pegmatite (Kfs = 23 crystals). Representative results are presented in Table 3.

Plagioclases of the Serra Branca granites have albitic composition ($\sim \text{An}_6\text{Ab}_{93}\text{Or}_1$), while the plagioclase from the Serra Negra granites have composition ranging from oligoclase to albite ($\text{An}_{0,5}\text{Ab}_{99}\text{Or}_{0,5} - \text{An}_{11}\text{Ab}_{88}\text{Or}_1$).

The K-feldspars from the Serra Negra and Serra Branca granites show similar compositions, ranging from $\text{An}_0\text{Ab}_5\text{Or}_{95}$ to $\text{An}_0\text{Ab}_7\text{Or}_{93}$ (Fig. 8A). However, the trace

element compositions show significant distinctions: the K-feldspars of the Serra Branca granites show higher Ba contents (72 – 4,400 ppm) compared to the feldspars from the Serra Negra granites ($\sim 3,400$ ppm) and the Serra Branca amazonite pegmatite (~ 447 ppm). The alkali feldspars from the Serra Branca granite and pegmatite have similar Cs contents (~ 940 ppm), and higher values compared to the Cs content recorded in the Serra Negra granites (~ 660 ppm). The amazonites from the Serra Branca amazonite pegmatite show a composition of $\sim \text{An}_0\text{Ab}_5\text{Or}_{95}$, high Rb ($\sim 5,212$ ppm), and

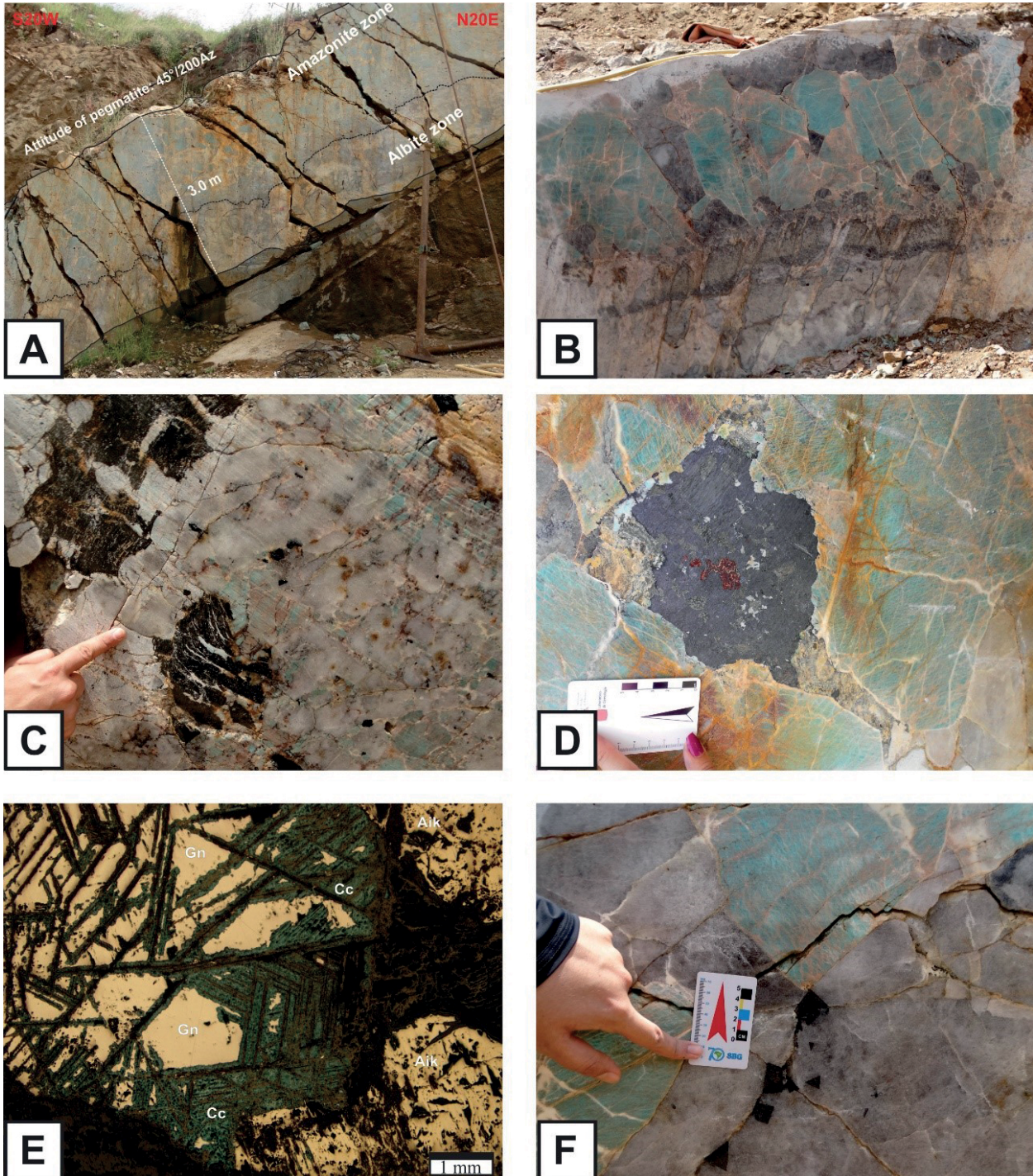


Figure 5. (A) The Serra Branca amazonite pegmatite dyke NW to WSW/45°; (B) Amazonite megacryst and quartz (amazonite zone) above the albite zone, showing irregular contact between them; (C) Biotite in the amazonite zone; (D) Aggregates of sulfides in the amazonite zone; (E) Galena (Gn) showing intergrowths of aikinite (Aik), and chalcocite (Cc) along the cleavage planes. (F) Rectangular and triangulate crystals of helvite hosted by quartz and amazonite megacrysts.

high to medium Pb (3,992 a 430 ppm) contents. Lead content in alkali feldspars is responsible for the bluish green color of the amazonites (Hofmeister & Rossman 1985, Ostrooumov & Banerjee 2005).

Opaque minerals

Thirteen grains of opaque minerals from the Serra Branca granites and nine grains from the Serra Negra granites were analyzed (Tab. 4). The opaque minerals recognized under reflected light from the Serra Negra granites are only magnetite (Fig. 8B), while those from the Serra Branca granites are

magnetite (the most abundant; Fig. 4D) and Mn-ilmenite, with MnO contents varying from 18.81 to 20.23wt.%. The analyzed magnetite from both plutons has low Cr_2O_3 (< 0.18wt.%) and V_2O_3 (< 0.25wt.%), similar trace element composition is presented by the Mn-ilmenites of the Serra Branca granites (Cr_2O_3 < 0.12wt.% e V_2O_3 < 0.631wt.%).

Titanite

Seven titanite crystals from the Serra Branca granites and four grains from the Serra Negra granites were analyzed. The results are shown in Table 5. The titanites from the Serra

Table 1. Chemical composition of biotite from the Serra Branca amazonite pegmatite, Serra Branca and Serra Negra granites.

Lithotypes Samples	Serra Branca granite			Serra Negra granite		Serra Branca amazonite pegmatite		
	AMZ 56	AMZ 74	AMZ 74A	AMZ 113	AMZ 114	AMZ 104P 1	AMZ 104P 2	AMZ 104P 3
Number of points analyzed = n	n = 6	n = 15	n = 27	n = 5	n = 10	n = 1	n = 1	n = 1
SiO ₂ (wt.%)	38.82	38.77	38.61	40.18	38.02	39.06	40.26	38.25
TiO ₂	1.48	2.13	2.15	1.15	1.34	1.15	1.57	1.78
Al ₂ O ₃	11.21	13.13	12.38	13.74	13.02	9.25	9.97	8.95
FeO	11.74	16.61	18.51	15.52	14.56	14.57	13.46	14.84
MnO	0.39	2.52	2.68	0.27	0.39	1.91	1.74	2.39
MgO	15.33	8.85	9.95	13.36	13.00	11.98	13.15	12.28
CaO	0.07	0.03	0.02	0.06	0.05	0.14	0.06	0.05
Na ₂ O	0.08	0.05	0.06	0.05	0.06	0.09	0.09	0.04
K ₂ O	9.40	8.33	9.55	8.84	9.40	8.40	9.03	8.92
SrO	0.00	0.00	0.00	0.00	0.00	0.00	0.00	0.00
BaO	0.10	0.06	0.08	0.07	0.10	0.00	0.07	0.03
F	1.96	3.09	2.90	1.43	1.51	4.76	5.25	4.76
Cl	0.01	0.01	0.01	0.01	0.01	0.05	0.00	0.01
Cr ₂ O ₃	0.05	0.02	0.04	0.03	0.04	0.05	0.00	0.00
NiO	0.01	0.02	0.04	0.02	0.02	0.06	0.00	0.00
Li ₂ O	0.03	0.04	0.01	0.00	0.03			
H ₂ O	2.86	2.32	2.47	3.28	3.08	1.39	1.31	1.40
Subtotal	93.71	96.58	99.53	98.17	94.82	95.14	97.71	95.60
O = F:Cl	0.83	1.30	1.22	0.60	0.64	2.02	2.21	2.01
Total	92.88	95.28	98.30	97.56	94.18	93.13	95.50	93.59
Si (apfu)	6.14	6.14	6.01	6.08	6.01	6.40	6.36	6.27
Al ⁺	1.86	1.86	1.99	1.92	1.99	1.60	1.64	1.73
Al ⁶⁺	0.23	0.59	0.29	0.53	0.43	0.19	0.21	0.00
Ti	0.18	0.25	0.25	0.13	0.16	0.14	0.19	0.22
Cr	0.01	0.00	0.00	0.00	0.00	0.01	0.00	0.00
Fe	1.55	2.20	2.41	1.96	1.92	2.00	1.78	2.04
Mn	0.05	0.34	0.35	0.03	0.05	0.26	0.23	0.33
Mg	3.61	2.09	2.31	3.01	3.06	2.93	3.09	3.00
Ni	0.00	0.00	0.00	0.00	0.00	0.01	0.00	0.00
Cu	0.00	0.00	0.00	0.00	0.00	0.01	0.00	0.00
Li	0.02	0.02	0.01	0.00	0.02	0.00	0.00	0.00
Ca	0.01	0.00	0.00	0.01	0.01	0.03	0.01	0.01
Na	0.03	0.02	0.02	0.01	0.02	0.03	0.03	0.01
K	1.90	1.68	1.90	1.71	1.89	1.76	1.82	1.87
Sr	0.00	0.00	0.00	0.00		0.00	0.00	0.00
Ba	0.01	0.00	0.01	0.00	0.01	0.00	0.00	0.00
OH	3.02	2.45	2.57	3.32	3.24	1.52	1.38	1.53
F	0.98	1.55	1.43	0.68	0.76	2.47	2.62	2.47
Cl	0.00	0.00	0.00	0.00	0.00	0.01	0.00	0.00
Total	19.61	19.27	19.56	19.43	19.60	19.55	19.53	19.67
Al ^{total}	2.09	2.45	2.27	2.45	2.42	1.79	1.85	1.73
Fe/Fe+Mg	0.30	0.51	0.51	0.39	0.39	0.41	0.36	0.40

apfu: atom per formula unit.

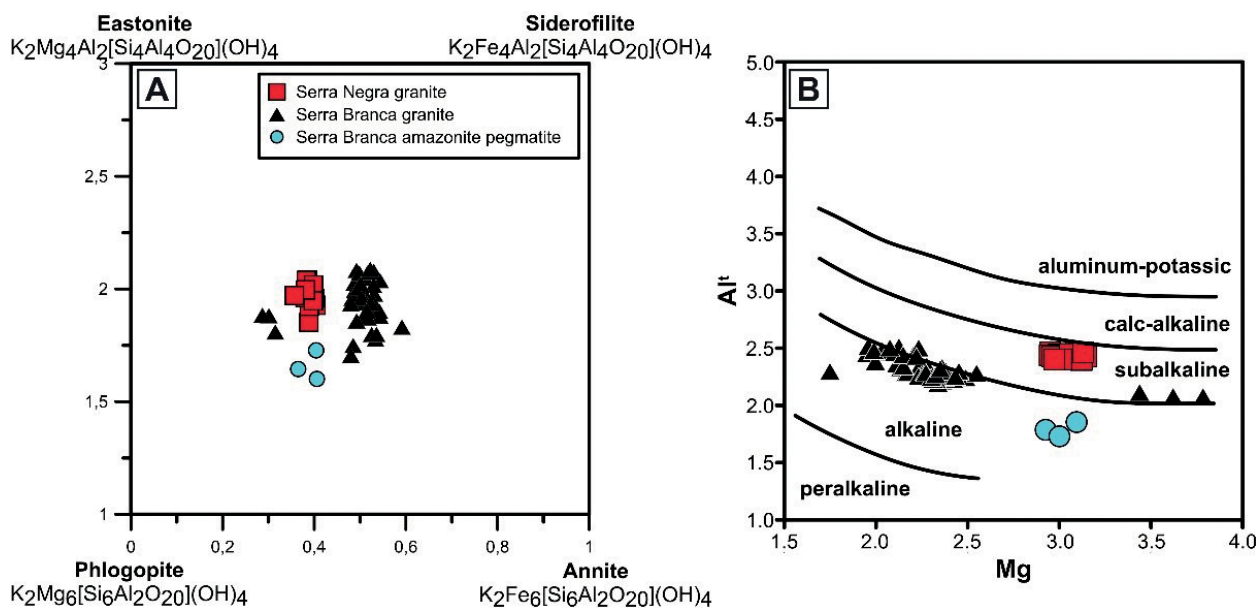


Figure 6. Biotite classification diagrams: (A) Fe# vs. Al^{IV} diagram from Deer (1992); B) Mg vs. Al^{IV} diagram from Nachit *et al.* (1985).

Table 2. Amphibole chemical composition of the Serra Branca and Serra Negra granites.

Lithotypes	Serra Branca granite				Serra Negra granite			
	Magmatic amphibole	Non magmatic amphibole			Magmatic amphibole	Non magmatic amphibole		
Type								
Samples	AMZ 55	Amz 55	Amz 56	AMZ 111	AMZ 113	AMZ 114	AMZ 113	AMZ114
Number of points analyzed = n	n = 19	n = 13	n = 24	n = 18	n = 1	n = 1	n = 12	n = 17
SiO ₂ (wt.%)	45.11	50.01	52.97	41.37	47.10	47.12	49.39	46.28
TiO ₂	0.15	0.12	0.17	0.23	0.92	0.86	0.41	0.59
Al ₂ O ₃	7.03	3.09	1.64	8.87	7.09	6.41	6.35	6.71
MnO	0.87	0.83	0.56	0.92	0.56	0.45	0.52	0.45
FeO	19.48	15.11	9.74	22.99	15.34	15.23	15.26	14.23
MgO	10.49	10.07	13.15	7.25	10.85	11.59	11.74	11.92
CaO	11.16	17.38	16.72	11.52	11.23	11.46	11.47	10.28
Na ₂ O	1.59	1.47	1.61	1.43	1.53	1.36	1.27	1.11
PbO	0.02	0.06	0.02	0.03	0.09	0.05	0.02	0.02
K ₂ O	1.32	0.52	0.21	1.46	0.79	0.86	0.73	1.75
F	1.09	0.42	0.26	0.54	0.51	0.70	0.52	0.69
Cl	0.01	0.01	0.01	0.01	0.02	0.00	0.01	0.01
Total	98.33	99.06	97.07	96.61	96.02	96.08	97.69	94.05
Si (apfu)	6.84	7.43	7.75	6.50	7.13	7.14	7.30	7.15
Al ⁴⁺	1.15	0.46	0.20	1.50	0.87	0.86	0.70	0.85
Ti	0.02	0.03	0.02	0.03	0.11	0.10	0.05	0.07
Al VI	0.11	0.24	0.19	0.15	0.40	0.29	0.41	0.39
Fe ³⁺	0.47	0.23	0.06	0.62	0.00	0.04	0.08	0.01
Fe ²⁺	2.00	1.82	1.19	2.40	1.94	1.89	1.83	1.70
Mg	2.37	2.23	2.87	1.70	2.45	2.62	2.59	2.75
Mn ²⁺	0.11	0.18	0.09	0.12	0.00	0.06	0.07	0.08
Ca	1.81	1.92	1.91	1.94	1.82	1.86	1.82	1.69
Na	0.10	0.10	0.20	0.03	0.18	0.13	0.17	0.08
Na	0.37	0.39	0.37	0.40	0.27	0.27	0.19	0.29
Pb	0.00	0.00	0.00	0.00	0.00	0.00	0.00	0.00
K	0.26	0.13	0.05	0.29	0.15	0.17	0.14	0.36
OH	1.47	1.79	1.87	1.73	1.75	1.67	1.75	1.66
F	0.53	0.53	0.27	0.27	0.24	0.33	0.24	0.34
Cl	0.00	0.00	0.00	0.00	0.00	0.00	0.00	0.00
Cations ^d	17.63	17.49	17.04	17.68	17.32	17.41	17.34	17.42

Apuf = atoms per formula unit.

Negra granites show Al₂O₃ ranging from 1.62 to 1.20wt.%, slightly higher than those recorded in titanites analyzed from the Serra Branca granites (0.87 to 1.25wt.%).

The titanite REE patterns, normalized to the chondrite (Nakamura 1974), are shown in Figure 9. The titanite from the Serra Negra Pluton is light rare earth elements (LREE) enriched compared to the titanite from the Serra Branca granites. In the La versus Sm (Fig. 10A) and Ce versus Yb (Fig. 10B) diagrams, the titanite from the Serra Branca granites shows lower Ce and Sm contents and similar La and Yb contents, compared to those of the Serra Negra granites.

CRYSTALLIZATION CONDITIONS

The crystallization conditions (pressure, temperature and oxygen fugacity) were determined using petrography, mineral chemistry and Zr contents in whole-rock geochemistry (Tab. 6). Magmatic amphibole (Czamanske & Wones 1973) and plagioclase in equilibrium with magmatic amphibole were used to define crystallization conditions.

Amphibole geothermobarometry

Studies carried on the paragenesis of calcic amphibole in mafic (meta-) igneous rocks (Spear 1981, Mader & Berman 1992, Ague & Brandon 1992, Ague 1997, Ernst & Liu 1998, Tulloch & Challis 2000) showed that with increasing pressure-temperature (P-T) conditions, calcic amphiboles exhibit an increase in Mg/(Mg + Fe) and K, Al, Na, and Ti contents and a decrease in Si and total Fe + Mg + Mn + Ca. Pressure conditions of crystallization, deduced from contact aureoles or

experimentally controlled runs, are linearly correlated with the Al_I content in magmatic amphibole. Many calibrations of the Al-in-amphibole barometer have been published (Hollister *et al.* 1987, Johnson & Rutherford 1988, Rutter *et al.* 1989, Blundy & Holland 1990, Schmidt 1992, Anderson & Smith 1995, Ernst & Liu 1998), since the pioneer work of Hammarstrom and Zen (1986).

Table 3. Feldspars composition of the Serra Branca amazonite pegmatite, Serra Branca and Serra Negra granites.

Lithotypes	Serra Branca granite	Serra Negra granite	Serra Branca amazonite pegmatite	Serra Branca granite	Serra Negra granite
	Alkali Feldspar			Plagioclase	
SiO ₂ (wt.%)	65.08	64.48	64.90	68.22	66.89
Al ₂ O ₃	17.27	17.06	16.81	18.99	20.59
FeO	0.08	0.03	0.13	0.17	0.07
CaO	0.01	0.01	0.01	1.05	2.46
Na ₂ O	0.73	0.52	0.59	10.75	10.12
K ₂ O	15.43	15.58	15.40	0.16	0.15
Total	99.44	98.40	98.76	99.75	100.50
Trace elements in ppm					
PbO	259.9	433.1	606.4	259.9	0.0
Cs ₂ O	943.2	660.3	943.2	848.9	0.0
Rb ₂ O	0.0	91.4	5212.1	0.0	0.0
BaO	4388.7	3493.1	447.8	358.3	358.3
An	0.02	0.07	0.05	6.04	11.74
Ab	7.22	4.83	5.46	93.01	87.43
Or	92.77	95.10	94.48	0.90	0.83

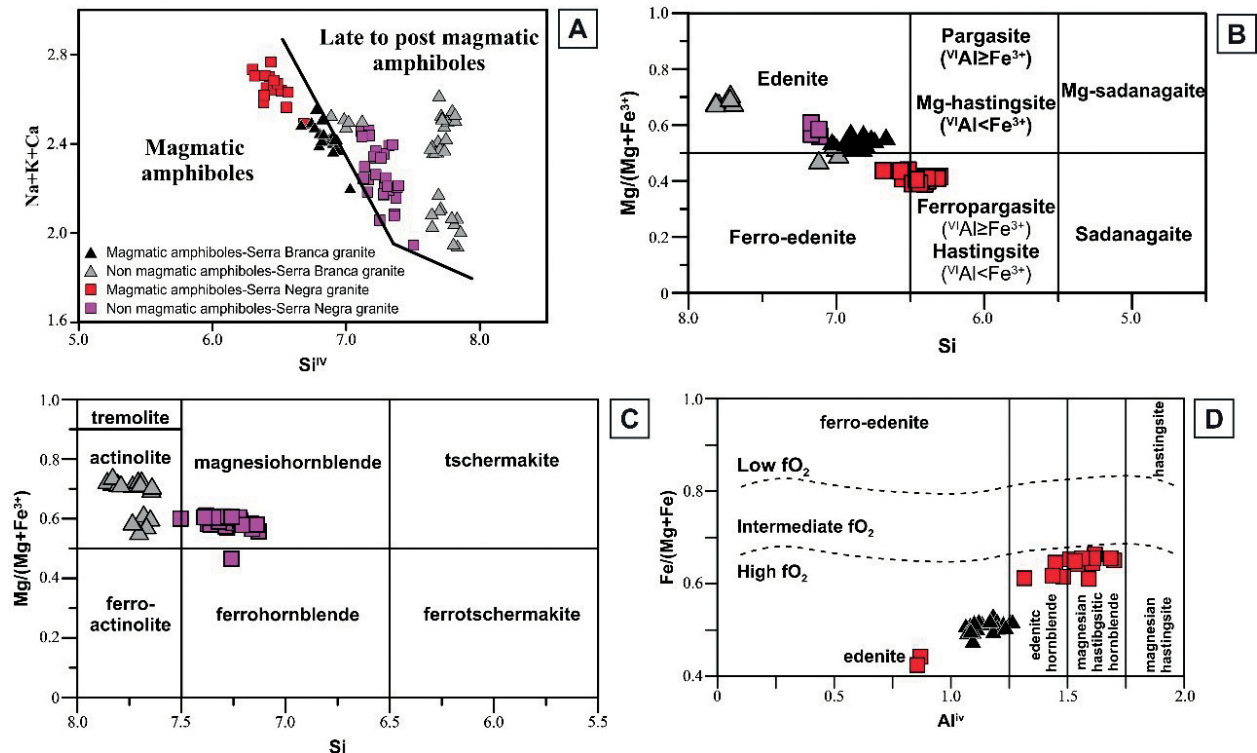


Figure 7. (A) Classification diagram of amphiboles Si^{IV} versus (Na + K + Ca) with fields defined by Czamanske and Wones (1973); (B) Amphibole classification diagram from Leake *et al.* (1997); (C) Amphibole classification diagram from Leake *et al.* (1997); (D) Al^{IV} vs Fe/(Mg+Fe) diagram with oxygen fugacity fields of Anderson & Smith (1995).

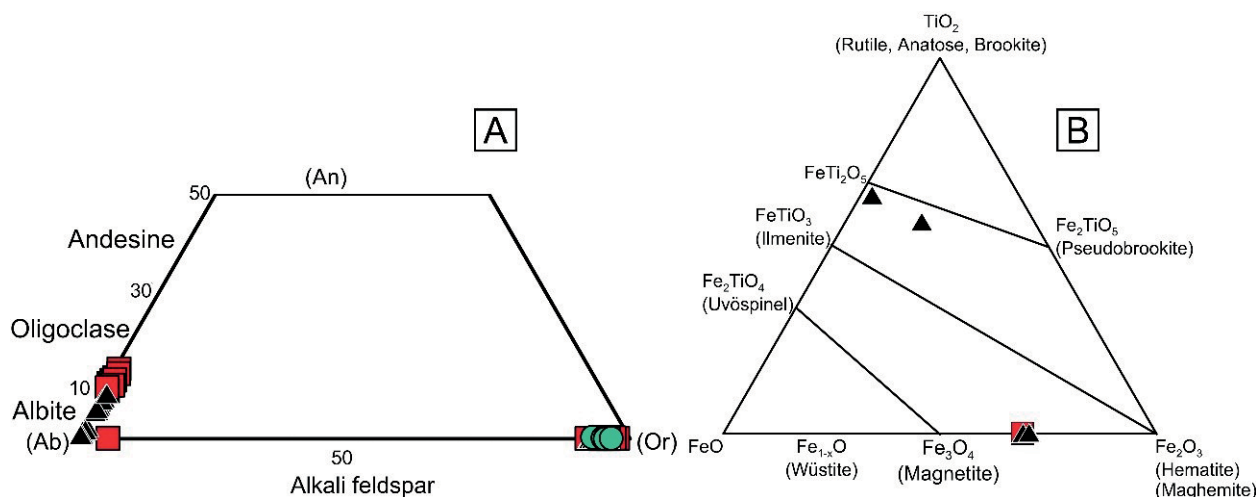


Figure 8. (A) An-Ab-Or ternary diagram for feldspar classification (Deer *et al.* 1992); (B) Fe_2O_3 vs FeO vs TiO_2 ternary diagram for oxides classification from Buddington & Lindsley (1964).

Table 4. Overall chemical composition of the Serra Branca and Serra Negra granites.

Lithotypes	Serra Branca granite	Serra Negra granite
SiO_2 (wt.%)	30.56	30.02
Al_2O_3	1.16	1.63
F	0.77	0.72
TiO_2	35.97	36.04
CaO	27.53	27.79
FeO	2.32	2.60
Total	98.32	98.81
Trace elements in ppm		
Er_2O_3	175	262
Tm_2O_3	175	0
Yb_2O_3	88	263
Ho_2O_3	524	436
Lu_2O_3	88	88
Dy_2O_3	0	349
Tb_2O_3	0	0
Sm_2O_3	259	1,121
Gd_2O_3	174	174
Eu_2O_3	86	345
ThO_2	281	187
Pr_2O_3	256	598
Nd_2O_3	979	1,957
Ce_2O_3	2,903	2,561
La_2O_3	1,023	512
UO_2	1,587	1,763
REE ^T	8,597	10,617

Table 5. Titanite chemical composition of the Serra Branca and Serra Negra granites.

Lithotypes	Serra Branca granite	Serra Negra granite
Cr_2O_3 (wt.%)	0.09	0.04
Al_2O_3	1.29	0.09
TiO_2	10.59	0.05
FeO	28.21	31.16
Fe_2O_3	53.19	69.68
MgO	0.04	0.02
MnO	4.80	0.14
NiO	0.01	0.00
V_2O_5	0.27	0.20
Total	98.48	101.40

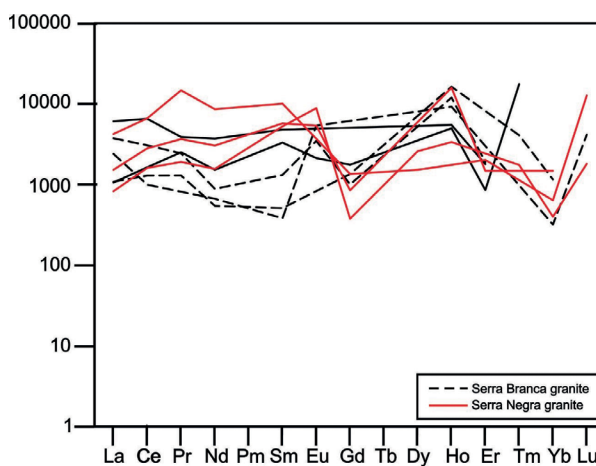


Figure 9. Rare earth elements contents of titanite crystals normalized to the chondrites values of Nakamura (1974).

The buffering equilibrium assemblage: quartz + hornblende + plagioclase (oligoclase or andesine) + K-feldspar + biotite + titanite + magnetite (or ilmenite) is required in calc-alkalic granites, in order to use the total Al-in-hornblende as a pressure crystallization indicator. This assemblage is present in the granites from the studied plutons, except by the albitic composition of the plagioclase recorded in the Serra Branca granites. Only amphibole with $\text{Fe}_t/(\text{Fe}_t + \text{Mg})$ ratio < 0.65 can be used in the Al-in-hornblende barometer (Anderson & Smith 1995). The $\text{Fe}_t/(\text{Fe}_t + \text{Mg})$ ratio of amphibole is in the range of 0.65–0.45 and 0.53–0.48 for the Serra Negra and Serra Branca granites, respectively.

Schmidt (1992) proposed an Al-in-amphibole barometer, experimentally calibrated under water-saturated conditions at pressures of 2.5–13 kbar, $f\text{O}_2 < \text{NNO}$ and temperatures of 700–655°C with a precision of 0.6 kbar [$P(0.6\text{kbar}) = 4.76\text{Al} - 3.01$]. Anderson and Smith (1995), using experimental data at ~675°C (Schmidt 1992) and at ~760°C (Johnson & Rutherford 1989), revised the calibration of Schmidt (1992) incorporating the effect of temperature,

obtained by the geothermometer plagioclase – amphibole: $P(\pm 0.6 \text{ kbar}) = 4.76 \text{Al}_{\text{Total}} - 3.01 - \{ [T(^{\circ}\text{C}) - 675] / 85 \} \times \{ 0.53 \text{Al}_{\text{Total}} + 0.00529 \times [T(^{\circ}\text{C}) - 675] \}$.

Using the Anderson and Smith (1995) geobarometer with crystallization temperatures obtained through the amphibole-plagioclase geothermometer, pressure in the 4.72–5.42 ± 0.6 kbar range were obtained for the crystallization conditions of the Serra Negra granites, while the Serra Branca granites crystallized at higher crust under pressures of 2.71–2.84 ± 0.6 kbar.

Geothermometer amphibole – plagioclase

The geothermometer amphibole – plagioclase can be used for granitic rocks when amphibole occurs in equilibrium with plagioclase. Blundy and Holland (1990), based on the reactions: edenite + 4quartz ↔ tremolite + albite and pargasite + 4quartz ↔ hornblende + albite, correlated the temperature with the Al^{IV} contents in amphibole and albite molecule in plagioclase. The use of the amphibole – plagioclase geothermometer is conditioned to the following rules: the amphibole should have Si < 7.8 apfu (atom per formula unit) and the plagioclase composition with An < 92%. Both conditions are

achieved by the Serra Negra and Serra Branca granites. The plagioclase – amphibole equilibrium temperatures, obtained through the Blundy and Holland (1990) geothermometer, were 666–670°C for the Serra Branca granite, and 711–751°C for the Serra Negra granite (Tab. 6).

Zircon saturation geothermometer

This geothermometer is based on the principle that Zr partition coefficients in crustal felsic magmas are a function of temperature (Watson 1979, Watson & Harrison 1983, 1984). Watson and Harrison (1983) established an equation to define the zircon crystallization temperatures, using the zircon contents in the whole-rock composition. Zircon saturation thermometer (Watson & Harrison 1983) defined temperatures within the 768–792°C range to the Serra Branca granites crystallization and 756–762°C to the Serra Negra granites crystallization (Tab. 6). The recorded temperatures are higher than those defined by the amphibole – plagioclase thermometer, which is expected, due the early crystallization of zircon, and are interpreted as the liquidus minimum temperature. On the other hand, the higher temperature can be caused by the presence of inherited zircon grains as have been reported from many plutons in the region.

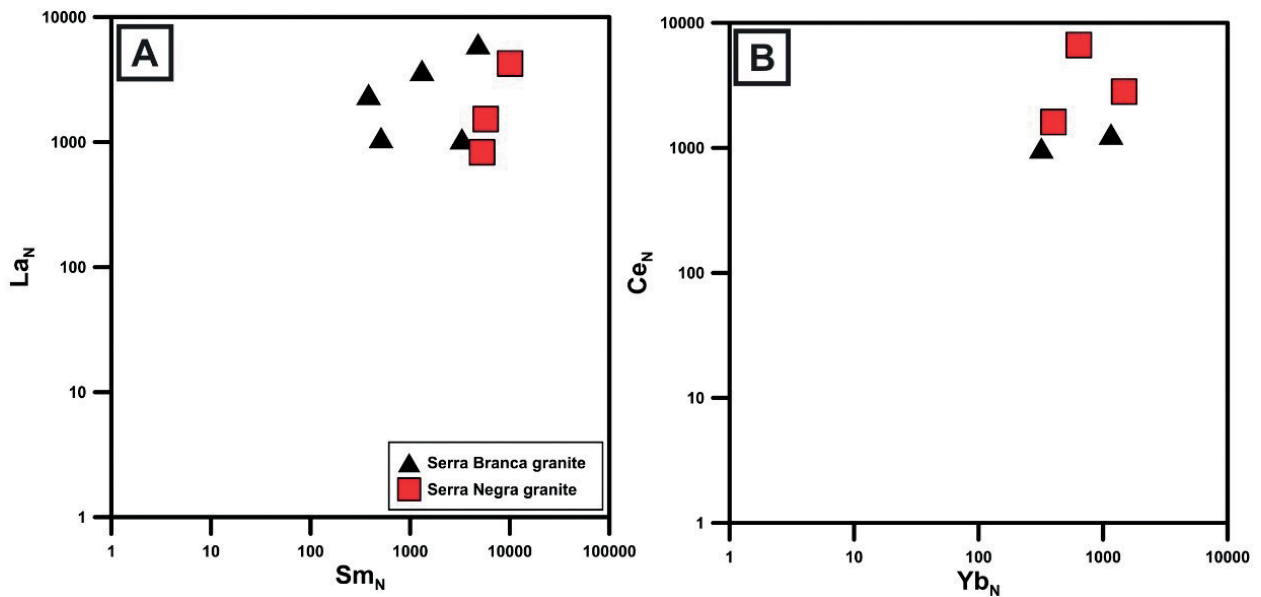


Figure 10. (A) Titanite crystals from the studied granites plotted on the La_N versus Sm_N diagram; (B) Titanite crystals from the studied granites plotted on the Ce_N versus Yb_N.

Table 6. Temperature and pressure data obtained from the amphibole-plagioclase geothermometer and zirconium saturation, and the total Al geobarometer in amphibole.

Lithotypes	Serra Branca granite				Serra Negra granite		
T (± 75°C)							
amphibole-plagioclase geothermometer	670°C	670°C	670°C	667°C	751°C	741°C	711°C
P (± 0.6 kbar)							
amphibole barometer	2.73 kbar	2.80 kbar	2.68 kbar	2.71 kbar	5.42 kbar	5.09 kbar	4.72 kbar
T °C							
Zr saturation geothermometer	793°C	768°C	776°C		763°C	756°C	773°C
LogfO ₂	-17.41	-17.39	-17.39	-17.51	-14.63	-14.94	-15.83

Oxygen fugacity

Oxygen fugacity is a magmatic source dependent (Loiselle & Wones 1979, Gill 1981, Wones 1989, Ishihara 1998), and it has an important influence on the liquidus temperature (Wones 1989) and therefor on, melt, mineral composition (Abbott & Clarke 1979, Abott 1985), magmatic process control, crystallization sequence, and types of crystallized minerals (Botcharnikov *et al.* 2005, France *et al.* 2010). According to Wones (1989), the equilibrium assemblage hedenbergite + ilmenite + oxygen ↔ titanite + magnetite + quartz is important in distinguishing relatively oxidized from relatively reduced granitic rocks. The equilibrium expression is expressed by $\log f_{O_2} = -30930/T + 14.98 + 0.142(P - 1)/7$, where T is the temperature (in kelvins) and P is the pressure (in bars). Occurrences of hedenbergite-rich clinopyroxene and ilmenite in granitic plutons imply oxygen fugacities like those required for the stability of fayalite. When the assemblage titanite + magnetite + quartz occurs with clinopyroxene or amphibole with intermediate or higher Mg/(Mg + Fe) ratios, a relatively high oxygen fugacity is implied.

The f_{O_2} values for the Serra Branca granites crystallization are in the 10^{-17} order, while the Serra Negra f_{O_2} values are in the order of 10^{-14} to 10^{-15} . The data suggests that both granites crystallized under high f_{O_2} , above the hematite buffer (Fig. 11), confirming the results obtained by the chemistry of amphibole.

U-Pb GEOCHRONOLOGICAL DATA

Zircon grains from two granitoid samples (AJ-94 - Serra Negra Pluton; AMZ-115 - Serra Branca Pluton) were selected to define the crystallization ages of the studied plutons. The rocks were initially crushed and sieved, and the grain separation was done through conventional gravimetric and magnetic methods.

U-Pb zircon analyses were carried out at the Geochronology Laboratory of the Universidade de Brasília using a Thermo-Fisher Neptune high-resolution multicollector ICP-MS coupled with a Nd: YAG UP213 New Wave laser ablation system, using the standard-sample bracketing method (Albarède *et al.* 2004). The GJ-1 standard zircon (Jackson *et al.* 2004)

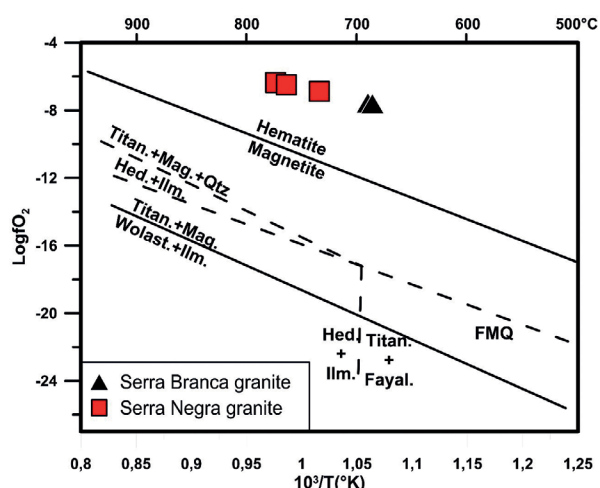


Figure 11. Oxygen fugacity of the studied granites obtained from the $\log f_{O_2}$ versus $10^3/T$ (°K) diagram (Wones 1989).

was used to quantify the amount of ICP-MS fractionation. The integration time was 1 s, and the ablation time was 40 s. A 25- μm spot size was used, and the laser settings were 10 Hz and 2–3 J/cm². $^{206}\text{Pb}/^{207}\text{Pb}$ and $^{206}\text{Pb}/^{238}\text{U}$ ratios were time corrected. Common ^{204}Pb was monitored using the ^{202}Hg and ($^{204}\text{Hg}/^{204}\text{Pb}$) masses. Common-Pb corrections were not done due to low signals for ^{204}Pb (< 30cps) and high $^{206}\text{Pb}/^{204}\text{Pb}$ ratios. The zircon standard 91500 (Jackson *et al.* 2004) was analyzed as an external standard.

Age calculations were performed using in-house developed Excel worksheets. Backscattered images were used to investigate the internal structures of individual zircon crystals prior to each analysis, in order to define the better grains and spot locations. Discordant ages were defined by $(1 - [^{206}\text{Pb}/^{238}\text{U} \text{ age}/^{207}\text{Pb}/^{206}\text{Pb} \text{ age}] * 100) > 10$.

Sample AJ-94

This sample is a biotite amphibole granite (6°32'52"S, 38°17'35"W). The zircon grains extracted from this granite are usually prismatic or square-like. Their lengths range from 50 to 150 μm and aspect length/width ratios range from 2:1 to 1:1. Almost all grains show oscillatory magmatic zoning and fractures (Fig. 12A). They exhibit forms with dominant presence of {211}, which, according to Corfu *et al.* (2003), are typical zircon crystal shapes of aluminous to calc-alkaline rocks.

Thirty-six spots on thirty grains were analyzed. All of them have $^{232}\text{Th}/^{238}\text{U}$ ratios > 0.2 which is typical of magmatic zircon (Williams & Claesson 1987). Sixteen spots were discarded due to discordance > 10, as also two analyzed spots due to high ^{204}Pb contents and other nine due to high analytical errors. Nine concordant analyses (Tab. 7) were used to build up a Discordia (Fig. 12B), which defined a Concordia age of

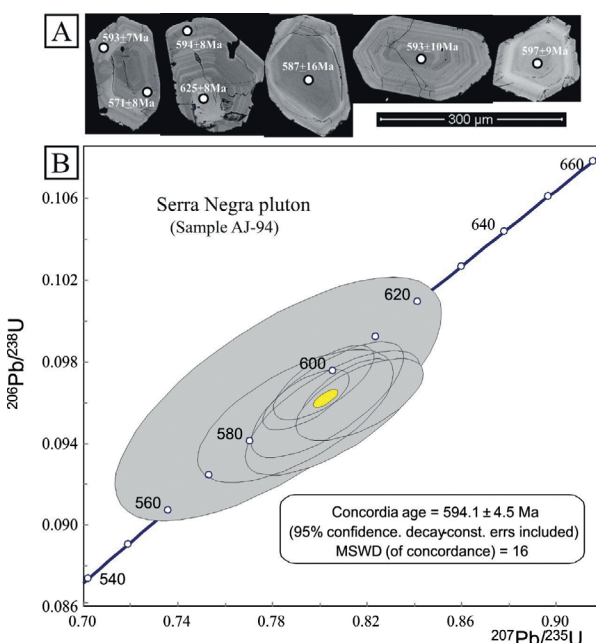


Figure 12. (A) Backscattered images of analyzed zircon grains of the Serra Negra granite and laser spot locations with their respectively $^{206}\text{Pb}/^{238}\text{U}$ ages; (B) Concordia diagram for the Serra Negra granite.

594 ± 4 Ma. This age is interpreted as the crystallization age of the Serra Negra granitoids. Cores and rims show similar ages and inherited cores and overgrowths were not recorded. The crystallization age defined to the Serra Negra granitoids is similar to those described in some high-K granitoids from the Transversal sub-province (Guimarães *et al.* 2004, Archanjo & Fetter 2004, Archanjo *et al.* 2008, among others).

Sample AMZ-115

This sample comprises a biotite amphibole monzogranite collected far away from the pegmatite (6°32'21.4"S, 38°16'45"W). The zircon grains are usually elongate, prismatic, with length ranging from 460 to 120 µm and length/width ratios from 4:1 to 2:1. Most of the grains show {100}

and {101} forms, which are typical zircon grain shapes of dry alkali and tholeiitic igneous rocks (Corfu *et al.* 2003).

Thirty grains were analyzed totaling thirty-four spots. The analyzed zircon grains are euhedral to subhedral and show igneous zoning (Fig. 13A). Inherited cores (Fig. 13A and Tab. 8) show Paleoproterozoic ²⁰⁷Pb/²⁰⁶Pb ages (2199 to 2147 Ma) and high ²³²Th/²³⁸U ratios (>2), reflecting an igneous source (Williams & Claesson 1987). The recorded ages associated to the ²³²Th/²³⁸U ratios suggest that these cores were inherited from the orthogneisses country rocks (Caicó Complex). The zircons with inherited core have rims with igneous zoning, concordant Neoproterozoic ages and high ²³²Th/²³⁸U ratios (Fig. 13B). Seven spot analyses were discarded due to high analytical errors and/or high ²⁰⁴Pb content.

Table 7. Summary of laser ablation inductively coupled plasma mass spectrometry (LA-ICP-MS) data of zircons from rock sample AJ-94 of the Serra Negra granites.

Grain spot	Isotopic ratios						Apparent ages							
	²⁰⁷ Pb/ ²⁰⁶ Pb	±(1σ)	²⁰⁷ Pb/ ²³⁵ U	±(1σ)	²⁰⁶ Pb/ ²³⁸ U	±(1σ)	²⁰⁷ Pb/ ²⁰⁶ Pb	±(1σ)	²⁰⁷ Pb/ ²³⁵ U	±(1σ)	²⁰⁶ Pb/ ²³⁸ U	±(1σ)	Rho	Th/U
ZR1N	0.06072	0.48	0.800	0.94	0.0955	0.71	629	21	597	8	588	8	0.76	1.191
ZR6	0.06046	1.07	0.804	1.66	0.0964	1.20	620	46	599	15	593	14	0.73	0.534
ZR11B	0.06087	0.54	0.810	0.96	0.0966	0.70	635	23	603	9	594	8	0.73	0.501
ZR12B	0.05977	0.57	0.794	0.93	0.0963	0.63	595	25	593	8	593	7	0.68	0.511
ZR13	0.06115	1.29	0.806	1.88	0.0955	1.31	645	55	600	17	588	15	0.70	0.319
ZR19N	0.06009	1.58	0.790	2.14	0.0953	1.39	607	67	591	19	587	16	0.65	0.832
ZR20	0.06147	0.99	0.817	1.36	0.0964	0.85	656	42	606	12	593	10	0.63	0.524
ZR27	0.05895	2.54	0.782	3.61	0.0962	2.53	565	109	587	32	592	29	0.70	0.633
ZR30	0.05990	0.67	0.801	1.08	0.0970	0.76	600	29	598	10	597	9	0.70	0.414

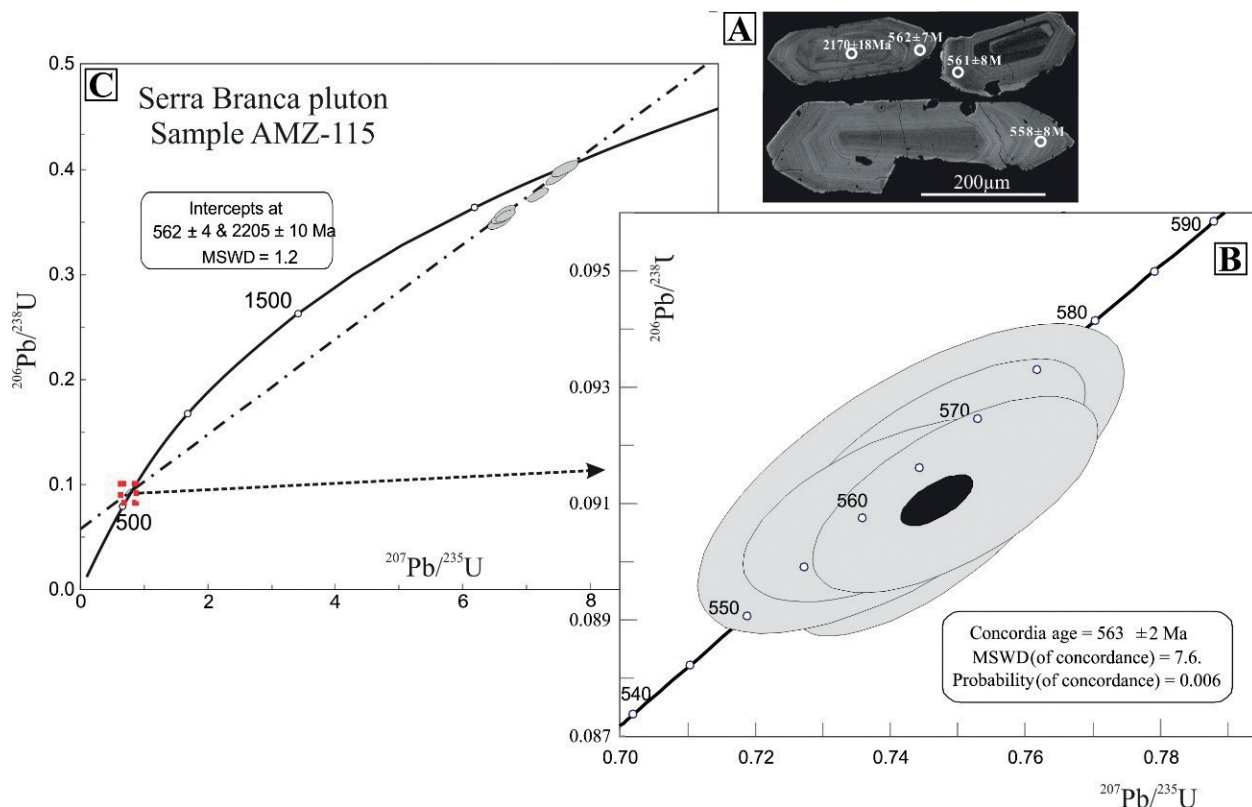


Figure 13. (A) Zircon SEM – CL pictures for analyzed zircon grains of the Serra Branca granite and laser spot locations with their respectively ages (²⁰⁷Pb/²⁰⁶Pb ages – Paleoproterozoic, ²⁰⁶Pb/²³⁸U ages – Neoproterozoic); (B) Zoom of the Neoproterozoic zircon cluster showed in (C); (C) Concordia diagram for all analyzed concordant zircon grains of the Serra Branca granite sample.

The analyzed spots defined two clusters in the Concordia diagram (Fig. 13C). The Discordia defines an upper intercept age of 2205 ± 10 Ma and an age of 562 ± 4 Ma in the lower intercept. The Neoproterozoic analyzed spots have a Concordia age of 563 ± 2 Ma, which is similar to that defined in the lower intercept, when all analyzed spots are considered. This age is interpreted as the crystallization age of the Serra Branca granitoids.

GEOCHEMISTRY

Nine samples were analyzed by ICP-AES for major elements and ICP-MS for trace elements, including samples of

granites from the Serra Negra and Serra Branca plutons and three samples from the Serra Branca amazonite pegmatite. Whole-rock chemical composition of pegmatites is not common worldwide due to the difficulties in obtain representative sample from rocks with large crystals and heterogeneities such as pegmatites (London 2008). Data from NYF- type pegmatite are even more scarce (Ercit 2005). In order to achieve the best representative samples of the Serra Branca amazonite pegmatite, a transversal sampling including albite and amazonite zones was done. The pegmatite sampling comprised 300 kg of $3.4 \times 0.2 \times 0.3$ m block. The sample was grinded and quarter, then milled down to 200 mesh and then subdivided in three samples for geochemical analyses. The results are shown in Table 9.

Table 8. Summary of laser ablation inductively coupled plasma mass spectrometry (LA-ICP-MS) data of zircons from rock sample AMZ-115 of the Serra Branca granites.

Grain spot	Isotopic ratios						Apparent ages						Rho	Th/U
	$^{207}\text{Pb}/^{206}\text{Pb}$	$\pm(1\sigma)$	$^{207}\text{Pb}/^{235}\text{U}$	$\pm(1\sigma)$	$^{206}\text{Pb}/^{238}\text{U}$	$\pm(1\sigma)$	$^{207}\text{Pb}/^{206}\text{Pb}$	$\pm(1\sigma)$	$^{207}\text{Pb}/^{235}\text{U}$	$\pm(1\sigma)$	$^{206}\text{Pb}/^{238}\text{U}$	$\pm(1\sigma)$		
ZR2N	0.13452	0.50	6.517	0.89	0.3514	0.63	2,158	17	2,048	16	1,941	21	0.71	0.550
ZR3B*	0.05972	0.63	0.745	1.07	0.0905	0.78	593	27	565	9	558	8	0.73	0.389
ZR4N	0.13773	0.55	7.158	0.96	0.3769	0.69	2,199	19	2,131	17	2,062	24	0.72	0.286
ZR5N	0.13459	0.75	6.595	1.09	0.3554	0.70	2,159	26	2,059	19	1,960	24	0.64	0.628
ZR5B*	0.05903	0.90	0.740	1.21	0.0909	0.71	568	39	562	10	561	8	0.59	0.325
ZR10	0.06071	0.88	0.791	1.18	0.0945	0.68	629	38	592	11	582	8	0.58	0.334
ZR11	0.06023	0.79	0.777	1.28	0.0936	0.94	612	34	584	11	577	10	0.73	0.257
ZR12N	0.13371	0.53	6.644	0.96	0.3604	0.71	2,147	19	2,065	17	1,984	24	0.74	0.551
ZR13	0.05839	2.10	0.745	2.81	0.0925	1.82	544	91	565	24	570	20	0.65	0.364
ZR17*	0.05893	1.21	0.743	1.74	0.0915	1.19	564	52	564	15	564	13	0.69	0.355
ZR19N	0.13711	0.65	7.588	1.10	0.4013	0.81	2,191	22	2,183	20	2,175	30	0.74	0.489
ZR20B	0.06046	0.55	0.778	1.03	0.0933	0.79	620	24	584	9	575	9	0.76	0.405
ZR27N	0.13734	0.45	7.474	1.01	0.3947	0.82	2,194	15	2,170	18	2,144	30	0.82	0.683
ZR27B*	0.05975	0.57	0.751	0.92	0.0911	0.61	595	25	569	8	562	7	0.67	0.573
ZR28	0.13513	0.55	6.643	0.93	0.3565	0.65	2,166	19	2,065	16	1,966	22	0.70	0.339
ZR29*	0.05962	0.79	0.750	1.15	0.0912	0.75	590	34	568	10	563	8	0.65	0.286
ZR30N	0.13563	0.76	6.545	1.13	0.3500	0.76	2,172	26	2,052	20	1,934	25	0.67	0.357
ZR30B*	0.05910	0.80	0.747	1.21	0.0916	0.83	571	35	566	10	565	9	0.69	0.469

*Zircons used to calculate the Concordia age diagram.

Table 9. Whole-rock chemical data performed by inductively coupled plasma mass spectrometry (ICP-MS) in the Serra Branca.

Lithotypes	Serra Negra granite			Serra Branca granite			Serra Branca amazonite pegmatite		
SiO ₂ (wt.%)	66.3	73.47	67.98	68.34	61.06	66.73	72.56	72.47	72.21
Al ₂ O ₃	16.56	13.67	15.49	16.06	16	18.18	14.88	14.87	15.01
Fe ₂ O ₃	2.19	1.87	2.28	2.17	4.8	2.02	0.29	0.28	0.28
MgO	0.37	0.68	1.26	0.39	1.72	0.57	0.04	0.02	0.03
CaO	2.01	1.65	1.94	1.26	2.93	1.45	0.04	0.04	0.04
Na ₂ O	3.69	4.91	4.53	5.07	4.71	8.74	3.31	3.42	3.4
K ₂ O	7.64	2.8	5.22	5.4	6.86	1.08	8.36	8.26	8.31
TiO ₂	0.19	0.15	0.26	0.2	0.43	0.23	0.02	0.01	0.01
P ₂ O ₅	0.06	0.08	0.15	0.09	0.34	0.07	< 0.01	< 0.01	< 0.01
MnO	0.07	0.03	0.04	0.04	0.09	0.23	0.02	0.02	0.02
F	0.02	0.05	0.06	0.06	0.07	0.19	0.03	0.02	0.02
Ba (ppm)	2,411	900	2,206	2,009	2,568	75	415	400	407
Be	1	8	2	9	7	34	50	42	40
Cs	12.7	2.8	3	4.1	5.6	50.6	131.8	129.4	129.5
Ga	17.5	17.9	18.4	20.4	19.7	38.1	52	53.3	50.4
Hf	3.3	3.2	3.8	4.5	3.1	4.9	2.4	14.5	2.3

Continue...

Table 9. Continuation.

Lithotypes	Serra Negra granite			Serra Branca granite			Serra Branca amazonite pegmatite		
Nb	6.6	5.7	8.5	10.4	7.3	50.5	56.5	74.5	34
Rb	211	97	153	216	200	271	3,004	2,994	3016
Sr	913	1096	1,280	1,429	1,420	508	217	210	213
Ta	0.5	0.4	0.7	0.7	0.5	1.7	8.2	11.5	5.6
Zr	113	104	127	160	121	132	17.5	117.8	12.1
Y	8.6	6	8.3	21.5	17.8	7.2	7.1	7.3	5.7
Cr	68	89	103	130	68	109	82	82	89
Cu	2.1	0.9	0.7	8.1	40.8	3	13.5	13	13.1
Pb	25.9	5.6	4.1	7.2	4.6	38.4	193	189.7	185.6
Zn	22	16	17	27	25	166	23	24	23
La	18.8	14.9	23.2	79	48.6	9.1	1	0.9	0.6
Ce	27.5	24.5	42.8	81.7	80.8	29.1	1.5	2.1	1.4
Pr	3.38	2.58	4.72	11.7	8.9	1.8	0.23	0.31	0.17
Nd	11.8	8.8	16.7	40.3	33.1	5.8	0.8	1.1	0.8
Sm	2.01	1.76	3.08	6.41	5.76	1.01	0.32	0.39	0.29
Eu	0.83	0.48	0.86	1.92	1.72	0.29	0.1	0.1	0.09
Gd	1.83	1.25	2.28	4.86	4.57	0.95	0.42	0.48	0.35
Tb	0.25	0.19	0.3	0.66	0.59	0.13	0.09	0.08	0.07
Dy	1.44	0.97	1.61	3.41	3.12	0.72	0.57	0.62	0.45
Ho	0.3	0.19	0.34	0.66	0.6	0.2	0.12	0.13	0.1
Er	0.94	0.54	0.78	1.65	1.65	0.64	0.46	0.55	0.33
Tm	0.14	0.08	0.12	0.26	0.23	0.11	0.08	0.12	0.07
Yb	0.93	0.56	0.78	1.55	1.46	0.95	0.8	1.21	0.54
Lu	0.13	0.1	0.12	0.2	0.22	0.19	0.13	0.23	0.11

The Serra Negra and Serra Branca granites and the Serra Branca amazonite pegmatite

The granitoids from the Serra Negra Pluton show higher SiO₂ contents (66 – 73wt.%) compared to those of the Serra Branca pluton (61 – 68wt.%). Granitoids from both plutons show high total alkalis (K₂O + Na₂O) contents and K₂O/Na₂O ratios > 1. According to the Shand's index the granitoids of the Serra Negra Pluton are metaluminous while those from Serra Branca range from metaluminous to slightly peraluminous (Fig. 14A). The Alumina Saturation Index (ASI = Al₂O₃/(CaO + Na₂O + K₂O) of the Serra Negra and Serra Branca granites varies from 1.2 to 1.4 and from 1.1 to 1.3, respectively.

The Serra Branca granitoids are alkaline while the Serra Negra granitoids plot in the calc-alkaline to alkaline (Fig. 14B) in the MALI (Na₂O + K₂O - CaO) versus SiO₂ diagram (Frost *et al.* 2001). The Serra Branca granitoids show Fe# [FeO_t/(FeO_t + MgO)] ranging from 0.85 to 0.74, and the Serra Negra granitoids show 0.86 to 0.64 values, both plotting in the magnesian field, except for two samples which fall in the ferroan field, in the SiO₂ versus (FeO_t/(FeO_t + MgO) diagram (Fig. 14C), with classification after Frost *et al.* (2001). The magnesian granitoids are associated to crystallization under high fO₂ condition while ferroan granitoids are crystallized under low fO₂ conditions.

The REE patterns of the Serra Negra granites, normalized to chondrite values of Nakamura (1974), are characterized by (Ce/Yb)_N ratios varying from 7.52 to 13.96 and absence of Eu anomalies (Fig. 15A). These patterns are similar to those recorded in the tonalitic orthogneisses of the Caicó Complex (Fig. 15A), except by higher contents of total REE in the Caicó

tonalitic orthogneisses, which can be explained by amphibole in the melting residue. The Serra Branca granites show REE patterns like those of the Serra Negra granites. One sample classified as medium to fine grained leucogranite, showed lower LREE and medium rare earth elements (MREE) contents compared to the two other samples. The REE patterns of the Serra Branca granites are like those of the Serra Negra granites, with similar (Ce/Yb)_N ratios (7.52 to 13.96), but have higher total REE concentration.

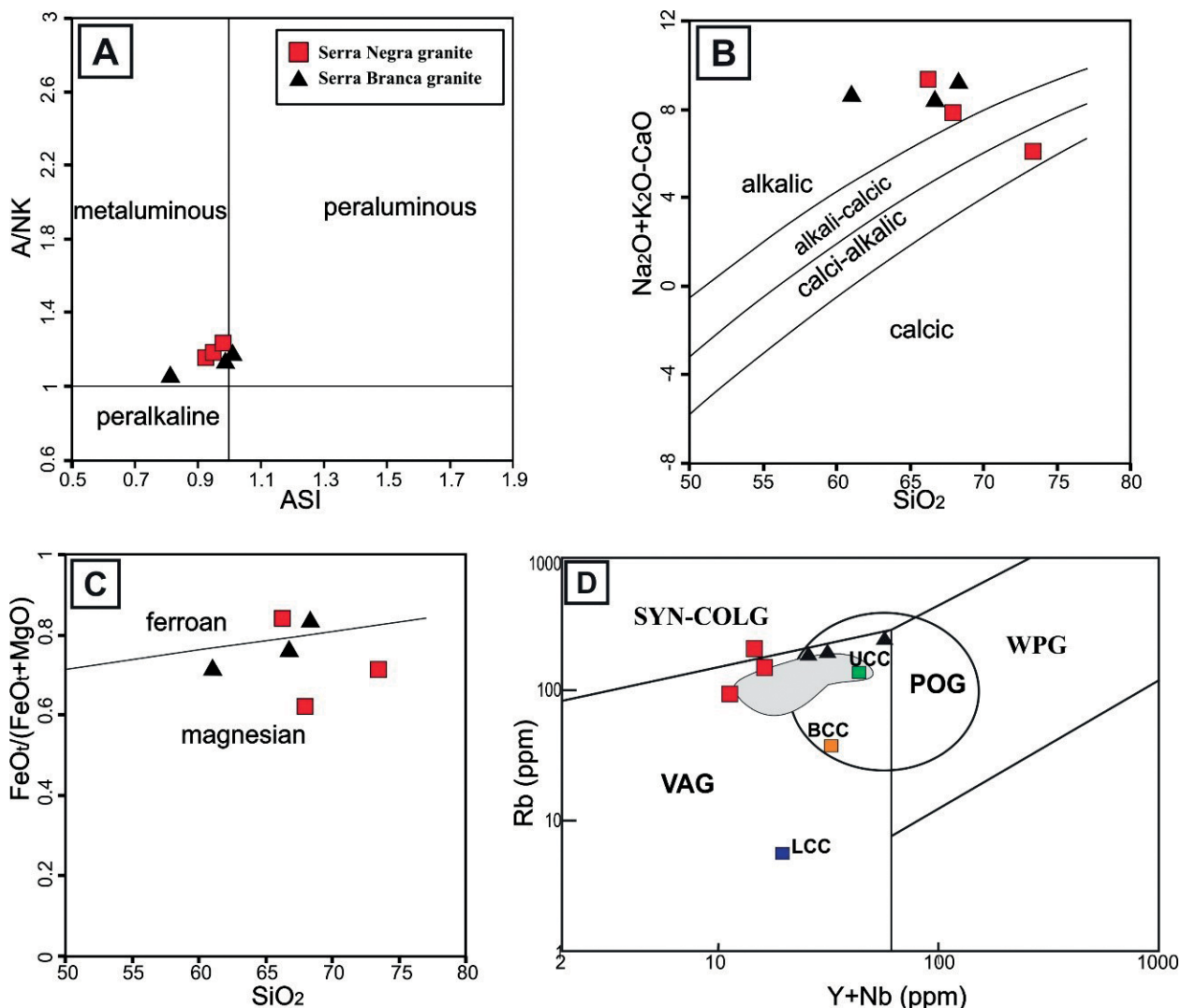
The Serra Branca amazonite pegmatite shows very low LREE contents, heavy rare earth elements (HREE) similar to those recorded in the Serra Negra and Serra Branca granitoids, and patterns characterized by Ce/Yb ratios < 1. The Serra Negra REE patterns are characterized by (Ce/Yb)_N ratios ranging from 7.52 to 13.96, with absent or positive Eu anomalies (Fig. 15A).

The spidergrams for the analyzed samples from the Serra Negra e Serra Branca granitoids are similar in shape, except by the higher LREE, K, Sr, P, Ti and Y contents in the Serra Branca granitoids patterns. On the other hand, the spidergram from the medium to fine grained leucogranite facies of the Serra Branca pluton is distinct from others Serra Branca and Serra Negra granitoids. This leucogranite facies is characterized by higher Cs, Rb, Pb, Nb, Ta, and lower Ba, K, Sr, P and LREE, being similar in shape to those recorded in the Serra Branca amazonite pegmatite (Fig. 15B).

In the tectonic setting discriminant diagrams of Pearce *et al.* (1984), the Serra Negra granites fall in the volcanic arc (VAG) and syn-collisional (syn-COLG) fields, and the Serra Branca granites fall in the VAG, syn-COLG and within plate

(WPG) fields. In the Pearce (1996) diagram, the Serra Branca granites fall within the Post-Orogenic granites (POG) field, while the Serra Negra granites fall in the VAG and syn-COLG fields. According to Pearce *et al.* (1990) and Pearce (1996), the trace elements composition of a melt generated by lithosphere zone undergoing melting can show either volcanic arc or

within plate character, depending on the previous geotectonic history. Besides that, crustal sources (lower, upper and bulk) have often a volcanic arc character (Fig. 14D). On the other hand, Y behaves as a compatible element during melting or fractional crystallization if there is a melt residue or crystallization assemblage involving amphibole and/or garnet. Thus, these



VAG: volcanic arc granite; POG: Post-Orogenic granites; WPG: within plate granite; SYN-COLG: syn-collisional.
Figure 14. (A) Studied rocks classification according to Shand's index (1943); (B) SiO_2 versus MALI ($\text{Na} + \text{K}_2\text{O} - \text{CaO}$) diagram (Frost *et al.* 2001); (C) Studied granites plotted on $\text{FeO}_t/(\text{FeO}_t + \text{MgO})$ versus SiO_2 diagram (Frost *et al.* 2001); (D) Tectonic discrimination diagram of Rb vs. (Y + Nb) (Pearce *et al.* 1984) for the studied granites (UCC: Composition of Upper Continental Crust, BCC: Composition of Bulk Continental Crust, LCC: Composition of Lower Continental Crust from Pearce (1996). The gray area represents the composition from the rocks of the Caicó complex).

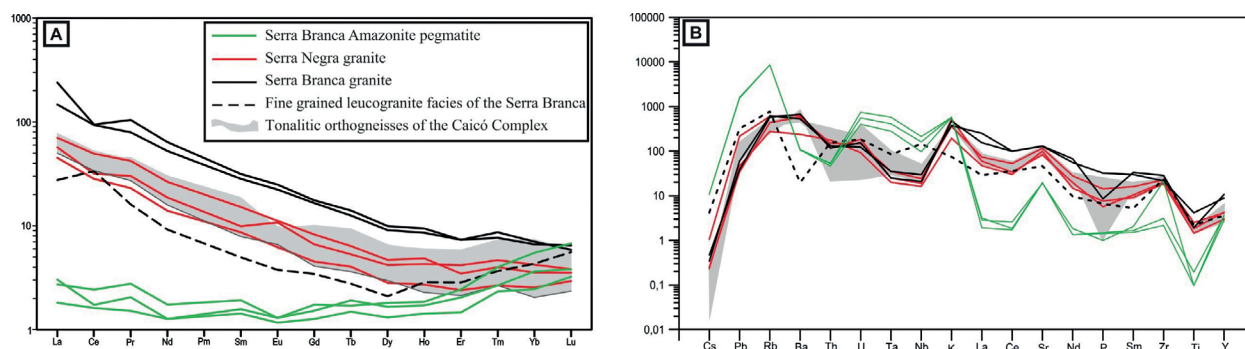


Figure 15. Selected chemical data of Serra Branca and Serra Negra granites, Serra Branca amazonite pegmatite and the Caicó Complex tonalitic orthogneiss: (A) REE pattern normalized by chondrite (Nakamura 1974); (B) Spidergram normalized to the chondrite (Sun 1980).

discriminant diagrams reflect the source composition and the processes involved during the magma evolution, rather than the setting in which the melt was generated and crystallized.

DISCUSSION

The field relationships and geochronological data show that the Serra Branca pluton is younger than the Serra Negra Pluton, and the amazonite pegmatite was intruded only into the Serra Branca granites. The Serra Negra pluton shows elongated shape, NE-SW-trending, magmatic foliation and S-C foliation, with C foliation plane aligned parallel to the NE-SW trending branch of the Lastro and Vieirópolis dextral shear zones, suggesting that the Serra Negra granitoids were emplaced syn- to late-transcurrence, 594 Ma ago, coeval with high-K granitoids described in the Transversal subprovince. The crystallization age (563 ± 2 Ma), defined for the granitoids of the Serra Branca Pluton, confirms the field relationships and dates the end of the transcurrence regime in the area.

The Serra Negra and Serra Branca granitoids show high SiO_2 and Al_2O_3 contents, and low compatible elements (MgO, Cr, Ni) contents, suggesting that their magma sources were crustal. The Serra Negra granitoids show trace element composition like those of the Caicó tonalitic orthogneisses (Fig. 15B), except by slightly higher Th and U contents, suggesting that the Serra Negra granitoids magma was generated by partial melting of a source geochemically similar to the Caicó tonalitic orthogneisses. A large percentage of melting from a source like the Caicó complex may explain the similarities between the trace elements composition of the Serra Negra granites and the Caicó orthogneisses and the absence of inherited zircon grains. The VAG signature of the Serra Negra granites is also an effect of their derivation from the Caicó orthogneisses, as shown in the Rb *versus* (Y + Nb) discriminant tectonic setting diagram (Pearce 1996), where the Caicó orthogneisses have a VAG signature (Fig. 14D). The detailed geochemical data presented by Souza *et al.* (2007) also shows that the Caicó tonalitic orthogneisses have a subduction-related signature. The presence of diorite enclaves hosted by the Serra Negra granites suggests that the necessary heating to promote the orthogneisses melting may have the influence of mafic magmas from the lithospheric mantle, ascending through the shear zones. However, isotopic data are necessary to confirm this hypothesis. The crystallization of the Serra Negra granitoids occurred at the medium crust (12 to 15 km) under high $f\text{O}_2$.

The Serra Branca granites are isotropic and post-transcurrence or post orogenic according to Pearce (1996) discriminant tectonic setting (Fig. 14D). The coarse-grained facies of the Serra Branca pluton are geochemically similar to the Serra Negra granitoids and Caicó orthogneisses, except by higher Na_2O , LREE, P and Ti contents, which suggests that the Serra Negra and Serra Branca granites share similar sources i.e., the Caicó orthogneisses. However, the trace element composition of the most differentiate facies (medium grained leucogranites) of the Serra Branca pluton is distinct from the coarse-grained facies by having higher incompatible element (F, Pb, Rb, Cs, Nb and Ta) contents and lower Ba, Sr, Y and LREE contents,

resembling in shape the trace element patterns of the Serra Branca amazonite pegmatite. During low degree of crustal melting at low-T conditions, or during fractional crystallization, Pb becomes strongly enriched in the melt relative to Ba and also relative to its source rock contents, because Pb is a more incompatible element. On the other hand, anatexis at high-T condition and large degree of partial melting produce melts less enriched in Pb and less depleted in Ba or even enriched relative to source rock (Finger & Schiller 2012).

The incompatible Pb behavior, associated to K-feldspar and/or plagioclase fractional crystallization, and low-T crystallization temperature of the Serra Branca granites explain the high Pb and lower Ba contents in the Serra Branca amazonite pegmatite. According to Martin (2004), efficient fractionation leads to NYF-type pegmatites, with peralkaline or metaluminous signature. Mildly peraluminous character can be developed in epizonal plutons due to alkali loss during degassing. The Serra Branca granites crystallized at depth between 7.8 and 9.5 km, under high $f\text{O}_2$ conditions, and are metaluminous to slightly peraluminous.

The evolution of the Serra Branca granites magma involved fractional crystallization of \pm K-feldspars, titanite, apatite and allanite (Fig. 16), leading to a melt enriched in incompatible elements (Cs, Pb, Rb, U, Ta, Nb) that crystallized as the leucogranite, and a residual melt even enriched in Pb and Rb, and LREE depleted. The melt continues fractionating apatite, titanite and allanite, resulting in a volatile rich product that finally crystallized as the amazonite pegmatite (Fig. 16). These variations, associated to the epizonal character of the Serra Branca pluton, provide evidence that the Serra Branca amazonite pegmatite resulted from extreme fractional crystallization of the Serra Branca granitic magma, which was generated by low degree of partial melting of a source similar to the Caicó orthogneisses, under high $f\text{O}_2$ condition and relatively low T conditions. The origin of the Serra Branca granitic magma by partial melting of orthogneisses of the Caicó Complex is supported by the presence of inherited Paleoproterozoic zircon cores in the Serra Branca granites (Fig. 13). The absence of inherited zircon grains in the Serra Negra granites may be explained by higher magma temperatures.

The Serra Branca amazonite pegmatite and its similarities with pegmatites worldwide

The classification of granitic pegmatites proposed by Černý and Ercit (2005) is the most accepted worldwide. This classification deals with geological location and divided the granitic pegmatites into five classes (abyssal, muscovite, muscovite – rare-element, rare-element and miarolitic), with most of them subdivided into subclasses taking under consideration geochemical and geological characteristics. This classification also divided the pegmatites of igneous sources into three families:

- NYF family with progressive accumulation of Nb, Y and F (besides Be, REE, Sc, Ti, Zr, Th and U), fractionated from subaluminous to metaluminous A- and I-type granites with crust or mantle contributions;

- LCT family with high Li, Cs and Ta (besides Rb, Be, Sn, B, P and F) contents, derived mainly from S-type granites, less commonly from I-type granites;
- mixed NYF + LCT.

The evidences for the Serra Branca amazonite pegmatite to be a NYF-type (Černý & Ercit 2005) are:

- lack of Al- and Li-rich mineral phases, which are typical in the mineral assemblage of LCT-type pegmatite, occurrence of pyrochlore, rutile and ilmenite (high field strength elements-rich mineral phases) and biotite which are typical mineral phases of NYF-type pegmatites (Wise 2017);
- high Nb, Y, F, Ta, Rb and Pb contents;
- amazonite megacrysts mineralization, which, according to Martin *et al.* (2008), is a rare pegmatite mineralization in a global level, and its occurrence is restrict to NYF-type pegmatite.

Wise (1999) proposed a classification of the NYF pegmatites, based on 40 occurrences of post-tectonic to anorogenic plutons emplaced at shallow levels into non-compressional environment. He divided the NYF pegmatites into three groups, based on the alumina saturation of the parental granite, as peralkaline, metaluminous and peraluminous. Each group was subdivided using characteristic mineralogical and geochemical features. The metaluminous group, as the

case of Serra Branca amazonite pegmatite, was subdivided in three subtypes:

- allanite subtype enriched in LREE (\pm Ti, Zr, F);
- euxenite subtype characterized by Nb > Ta, Ti, Zr, Y, P, LREE to HREE minerals;
- the gadolinite subtype, with Be, Y + HREE, Nb > Ta, Ti, Zr, P, and F.

The Serra Branca amazonite pegmatite have moderate Be (40 to 50 ppm) contents, Be-bearing mineral phases (hervine and phenakite) within the amazonite zone and HREE contents higher than LREE contents, which characterizes the studied pegmatite as a gadolinite subtype.

According to Černý and Ercit (2005), the NYF-type pegmatites are associated to metaluminous I- (syn-, tardi- to post-orogenic, NYF-I) and A-type granitoids (anorogenic, NYF-A). The Serra Branca amazonite pegmatite are likely from NYF-I subtype, due its derivation from the I-type Serra Branca granites, originated from partial melting of orthogneisses of the Caicó Complex.

Whole-rock geochemical data for NYF pegmatites is rare in the literature. However, some data, available for NYF-type pegmatites without amazonite mineralization from the Hearne Province in northern Saskatchewan, Canada (McKeough *et al.* 2013), and three others, one amazonite pegmatite and two without amazonite mineralization, from Evje-Iveland, Norway

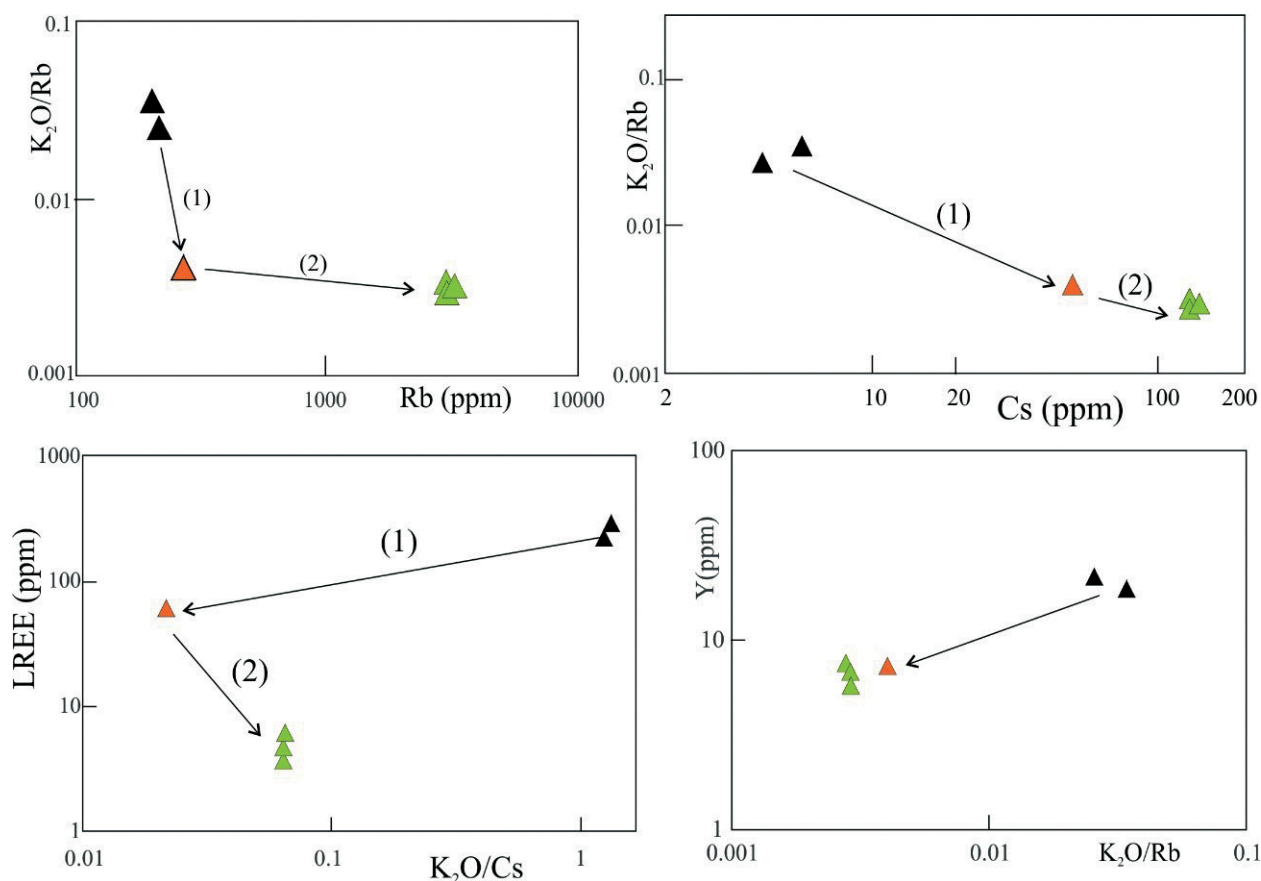


Figure 16. Selected variation diagrams (A) K_2O/Rb vs Rb ; (B) K_2O/Rb vs Cs ; (C) $LREE$ vs K_2O/Cs ; (D) Y vs K_2O/Rb , showing the magma evolution of the Serra Branca granites and amazonite pegmatites for a fractional crystallization of (1) $\pm K$ -feldspars, titanite, apatite and allanite; (2) apatite, titanite and allanite. Legend: Serra Branca granite (black triangle), fine-grained leucogranite facies of the Serra Branca granites (orange triangle), and Serra Branca amazonite pegmatite (green triangle).

(Snook 2014), were used to compare with the Serra Branca amazonite pegmatite. The pegmatites from the Hearne Province is divided into two groups: hybrid pegmatites and simple pegmatites. The hybrid pegmatites represent complex-type hybridized pegmatites, due to metasomatic interaction with the host rocks (McKeough *et al.* 2013).

The Serra Branca amazonite pegmatite shows REE patterns very distinct from both pegmatite groups of the Hearne Province and Evje-Iveland (Fig. 17). The REE pattern of the Serra Branca amazonite pegmatite are characterized by very low REE contents mainly LREE, with LREE/HREE ratios > 1. On the other hand, the REE patterns of pegmatites from the Hearne Province and Evje-Iveland show deep negative Eu anomalies, and most of them have LREE/HREE ratios ~1,

The Serra Branca amazonite pegmatite spidergrams (Fig. 18) normalized to the Sun (1980) chondrite values are distinct from both the Evje-Iveland and those of the Hearne Province pegmatites by lower Th, U, LREE, P and higher Cs, Rb, Pb contents. Besides that, the Serra Branca amazonite pegmatite is geochemically distinct from the Evje-Iveland pegmatite by peak at Sr, lower Ti, and higher Ba, K, Nb and Ta contents (Fig. 18). The pegmatites from Evje-Iveland share similar incompatible elements patterns, except by lower contents of Ba and Sr recorded in the amazonite mineralized pegmatite.

The simple pegmatites of the Hearne Province show a geochemical uniform behavior, and lower Ta and Nb and higher Ti contents compared to the Serra Branca amazonite pegmatite.

The hybrid Hearne Province pegmatites show distinct incompatible element patterns. Compared to the Serra Branca amazonite pegmatite, the Hearne Province pegmatites show higher and lower Ti, Sr, Nb, Ta and Ba contents, but are always U-, and Th-rich and Cs, Pb, Rb and Ba depleted. It suggests that metasomatic interaction with the host rocks was not a process involved in the Serra Branca amazonite pegmatite magma evolution.

CONCLUSIONS

The Serra Negra and Serra Branca granitoids resulted from distinct degree of partial melting of similar sources, and have crystallization ages 594 ± 4 Ma and 563 ± 2 Ma, respectively. The Serra Negra granites were emplaced syn- to tardi- transcurrent events, associated to the Lastro and Vieirópolis shear zones, and crystallized in the middle crustal levels under higher fO_2 conditions and temperatures within the 711–751°C interval.

The Serra Branca granites are post-transcurrent (post-orogenic), emplaced at shallower levels, under high fO_2 . The Serra Branca granitic magma evolved by fractional crystallization of \pm K-feldspar, titanite, allanite, apatite leading to melts rich in incompatible elements, the Serra Branca leucogranitic facies, and the Serra Branca amazonite pegmatite.

The Serra Branca amazonite pegmatite is the first pegmatite characterized mineralogically and geochemically as a NYF-type gadolinite subtype within the BP and comprise rare pegmatites with economic importance outside the Seridó

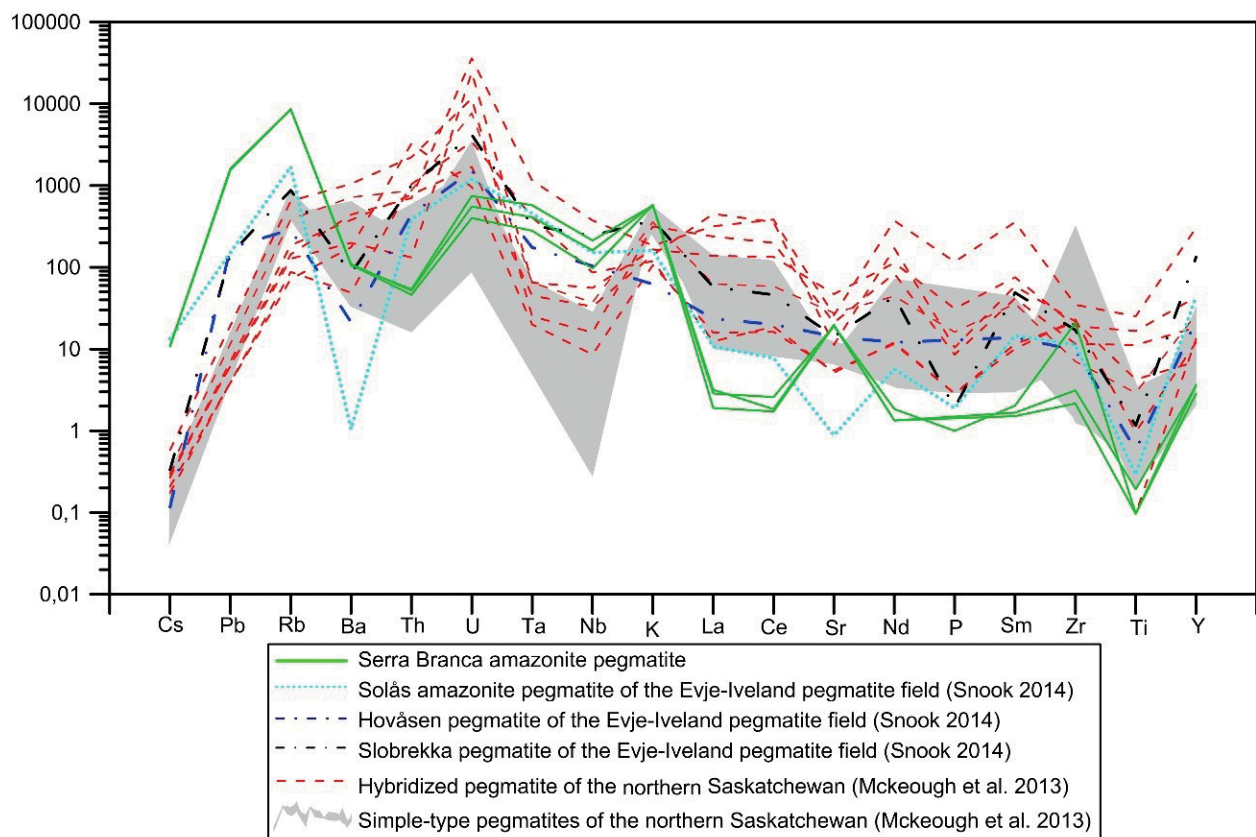


Figure 17. Comparison of spidergrams for the Serra Branca amazonite pegmatite, pegmatites of the Evje-Iveland pegmatite field (Snook 2013) and the simple and hybrid pegmatites from the Northern Saskatchewan (McKeough *et al.* 2013) normalized to the chondrite values of Sun (1980).

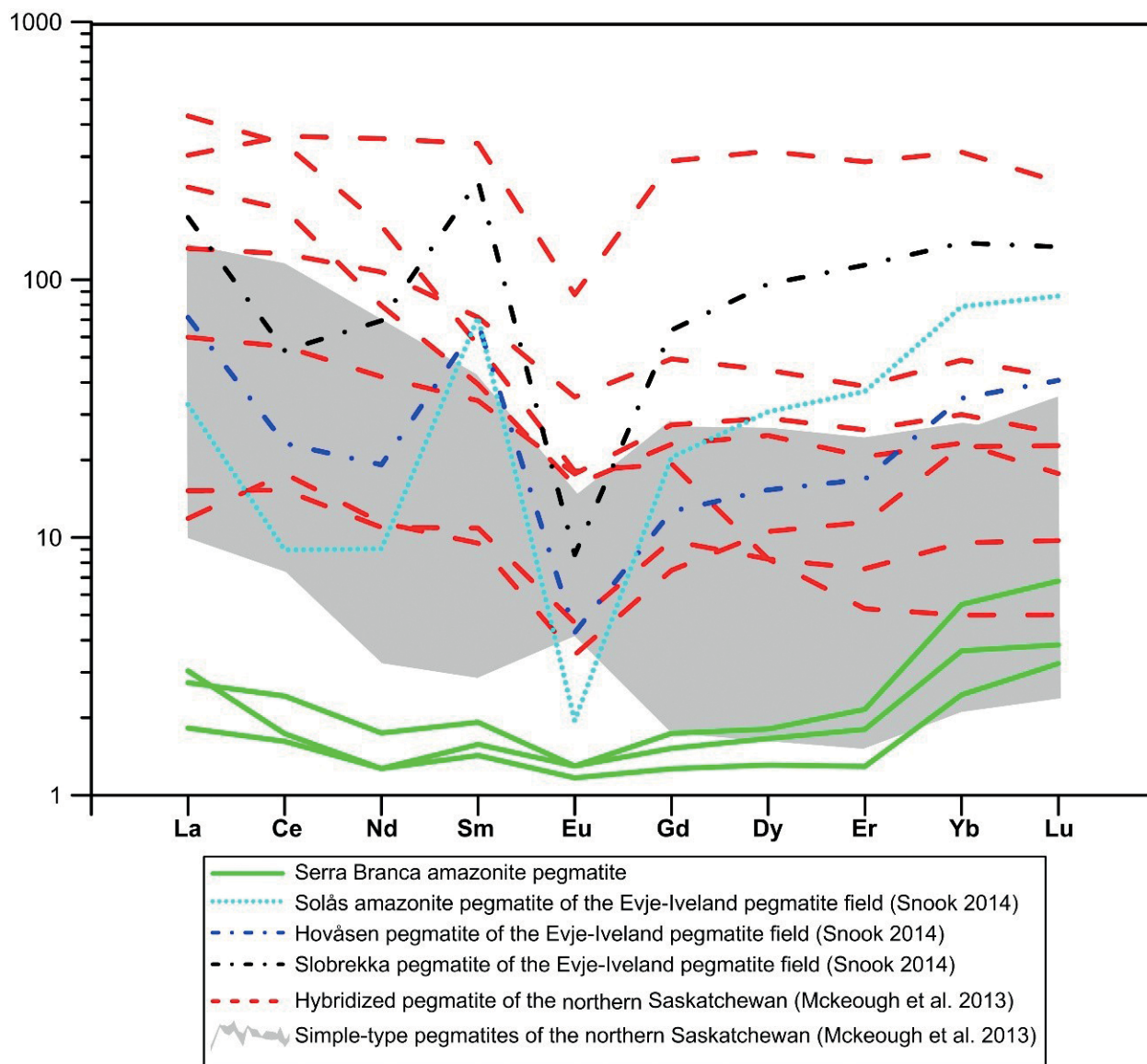


Figure 18. Rare earth elements (REE) pattern from the Serra Branca amazonite pegmatite, pegmatites of the Evje-Iveland pegmatite field (Snook 2013) and the simple and hybrid pegmatites from the Northern Saskatchewan (McKeough *et al.* 2013) normalized to the chondrite values of Nakamura (1974). Symbols as in Figure 15.

Pegmatite Province. They constitute, worldwide, a geochemically unique pegmatite occurrence of NYF type, due their low LREE, high Pb and Rb contents.

ACKNOWLEDGMENTS

We are grateful to the GRANISTONE S/A company for providing support to our research and for the supply

of pegmatite samples. We also thank the Coordenação de Aperfeiçoamento de Pessoal de Nível Superior (CAPES) for scholarships granted to Igor Manoel Belo de Albuquerque e Souza, Glenda Lira Santos and José Ferreira de Araújo Neto. We would like to express our gratitude to Dr. Axel Müller for his general assistance with this research. We also thank Professor Dr. Nilson Botelho (Universidade de Brasília, Brazil) for the electron microprobe analysis.

ARTICLE INFORMATION

Manuscript ID: 20190083. Received on: 08/31/2019. Approved on: 02/21/2020.

I.M.B.A.S. wrote the first manuscript draft, worked on sample preparation, analysis and interpretation, drew most of the figures and prepared all tables; I.P.G. worked on the interpretation of the geochronological data, whole-rock and mineral chemistry data, gave support in all chapters of the manuscript, and drew some figures (12 and 13); S.B.B. participated in the field work, sample collecting, provided support and advisement regarding whole-rock and pegmatite descriptions and interpretations; G.L.S. participated of the field work, sample preparation, chemical and mineralogical interpretation of the pegmatite, and contributed to text reviewing; J.F.A.N. helped with field geology, petrographic descriptions and text reviewing.

Competing interests: The authors declare no competing interests.

REFERENCES

- Abbot R.N. 1985. Muscovite-bearing granites in the AFM liquidus projection. *Canadian Mineralogist*, **23**:553-561.
- Abbott R.N., Clarke D.B. 1979. Hypothetical liquidus relationships in the system Al_2O_3 -FeO-MgO projected from quartz, alkali feldspar and plagioclase, a(H₂O) < 1. *Canadian Mineralogist*, **17**:549-560.
- Ague J.J. 1997. Thermodynamic calculation of emplacement pressures for batholithic rocks, California: Implication for the aluminum-in-hornblende barometer. *Geology*, **25**(6):563-566. [https://doi.org/10.1130/0091-7613\(1997\)025%3C0563:TCOEPF%3E2.3.CO;2](https://doi.org/10.1130/0091-7613(1997)025%3C0563:TCOEPF%3E2.3.CO;2)
- Ague J.J., Brandon M.T. 1992. Tilt and northward offset of Cordilleran batholiths resolved using igneous barometry. *Nature*, **360**:146-149. <https://doi.org/10.1038/360146a0>
- Albarède F., Telouk P., Blichert-Toft J., Boyet M., Agrancier A., Nelson B. 2004. Precise and accurate isotopic measurements using multiple-collector ICPMS. *Geochimica et Cosmochimica Acta*, **68**(12):2725-2744. <https://dx.doi.org/10.1016/j.gca.2003.11.024>
- Almeida F.F.M., Hasui Y., Brito Neves B.B., Fuck R. 1981. Brazilian structural provinces: an introduction. *Earth Science Reviews*, **17**(1-2):1-29. [https://doi.org/10.1016/0012-8252\(81\)90003-9](https://doi.org/10.1016/0012-8252(81)90003-9)
- Anderson J.L., Smith D.R. 1995. The effects of temperature and fO₂ on the Al-in-hornblende barometer. *American Mineralogist*, **80**(5-6):549-559. <https://doi.org/10.2138/am-1995-5-614>
- Araújo Neto J.F., Lira Santos G., Souza I.M.B.A., Barreto S.B., Santos L.C.M.L., Bezerra J.P.S., Carrino T.A. 2018. Integration of remote sensing, airborne geophysics and structural analysis to geological mapping: a case study of the Vieirópolis region, Borborema Province, NE Brazil. *Geologia USP. Série Científica*, **18**(3):89-103. <https://doi.org/10.11606/issn.2316-9095.v18-140834>
- Archanjo C.J., Fetter A. 2004. Emplacement setting of the granite sheeted pluton of Esperança (Brasiliano orogen, Northeastern Brazil). *Precambrian Research*, **135**(3):193-215. <http://dx.doi.org/10.1016/j.precamres.2004.08.008>
- Archanjo C.J., Hollanda M.H.B.M., Rodrigues S.W.O., Brito Neves B.B.B., Armstrong R. 2008. Fabrics of pre- and syntectonic granite plutons and chronology of shear zones in the Eastern Borborema Province, NE Brazil. *Journal of Structural Geology*, **30**(3):310-326. <http://dx.doi.org/10.1016/j.jsg.2007.11.011>
- Barreto S.B., Muller A., Araujo Neto J.F., Bezerra J.P.S., Souza I.M.B.A., França R.H.M., Santos L.C.M.L. 2016. Vieirópolis Pegmatite Field, Northwest of Paraíba State, Brazil: New Occurrences of Amazonite Pegmatites. In: Jacobson M.I. (ed.), *Second Eugene E. Foord Pegmatite Symposium: Abstracts, Short Papers, Posters and Program*. Denver, Friends of Mineralogy, Colorado Chapter, p. 24-26.
- Beurlen H., Da Silva M.R.R., Thomas R., Soares D.R., Olivier P. 2008. Nb-Ta-(Ti-Sn)-oxide mineral chemistry as tracers of rare-element granitic pegmatite fractionation in the Borborema Province, Northeast Brazil. *Mineralium Deposita*, **43**(2):207-228. <http://dx.doi.org/10.1007/s00126-007-0152-4>
- Beurlen H., Rhede D., Da Silva M.R.R., Thomas R., Guimaraes I.P. 2009. Petrography, Geochemistry and Chemical Electron Microprobe U-Pb-Th dating of Pegmatitic Granites in Borborema Province, Northeastern Brazil: a Possible Source of Rare Element Granitic Pegmatites. *Terra*, **6**(1):59-71.
- Blundy J.D., Holland T.J.B. 1990. Calcic amphibole equilibria and a new amphibole plagioclase geothermometer. *Contributions to Mineralogy and Petrology*, **104**:208-224. <https://doi.org/10.1007/BF00306444>
- Botcharnikov R.E., Koepke J., Holtz F., McCammon C., Wike M. 2005. The effect of water activity on the oxidation and structural state of Fe in a ferro-basaltic melt. *Geochimica et Cosmochimica Acta*, **69**(21):5071-5085. <https://doi.org/10.1016/j.gca.2005.04.023>
- Brito Neves B.B., Santos E.J., Van Schmus W.R. 2000. Tectonic History of the Borborema Province. In: Cordani U.G., Milani E.J., Thomaz Filho A., Campos D.A. (eds.), *Tectonic Evolution of South America*. Rio de Janeiro, 31st. *International Geological Congress*, p. 151-182.
- Buddington A.F., Lindsley D.H. 1964. Iron-titanium oxide minerals and synthetic equivalents. *Petrology*, **5**(2):310-357. <https://doi.org/10.1093/petrology/5.2.310>
- Černý P. 1991a. Fertile granites of Precambrian rare-element pegmatite fields: is geochemistry controlled by tectonic setting or source lithologies? *Precambrian Research*, **51**(1-4):429-468. [https://doi.org/10.1016/0301-9268\(91\)90111-M](https://doi.org/10.1016/0301-9268(91)90111-M)
- Černý P. 1991b. Rare-element granitic pegmatites. Part 1: Anatomy and internal evolution of pegmatite deposits. Part 2: Regional to global environments and petrogenesis. *Geoscience Canada*, **18**(2):49-81.
- Černý P., Ercit T.S. 2005. The classification of granitic pegmatites revisited. *The Canadian Mineralogist*, **43**(6):2005-2026. <https://doi.org/10.2113/gscanmin.43.6.2005>
- Corfu F., Hancher J.M., Hoskin P.W.O., Kinny P. 2003. Atlas of zircon textures. *Reviews in Mineralogy and Geochemistry*, **51**(1):469-500. <https://doi.org/10.2113/0530469>
- Czamanske G.K., Wones D.R. 1973. Oxidation during magmatic differentiation, Finnmarks Complex, Oslo Area, Norway: Part 2, the mafic silicate. *Journal of Petrology*, **14**(3):349-380. <https://doi.org/10.1093/petrology/14.3.349>
- Da Silva M.R.R., Höll R., Beurlen H. 1995. Borborema Pegmatitic Province: geological and geochemical characteristics. *Journal of South America Earth Sciences*, **8**(3-4):355-364. [https://doi.org/10.1016/0895-9811\(95\)00019-C](https://doi.org/10.1016/0895-9811(95)00019-C)
- Dantas E.L. 1997. *Geocronologia U-Pb e Sm-Nd de terrenos arqueanos e paleoproterozoicos do Maciço Caldas Brandão, NE do Brasil*. Thesis, Instituto de Geociências e Ciências Exatas, Universidade Estadual Paulista, Rio Claro, 208 p.
- Deer W.A., Howie R.A., Zussman J. 1992. *An Introduction to the Rock Forming Minerals*. 2nd ed. London, Longman, 696p.
- Ercit T.S. 2005. REE-enriched granitic pegmatites. In: Linnen R.L., Samson I.M. (eds.), *Rare-Element Geochemistry and Mineral Deposits*. *Geological Association of Canada, Short Course Notes*. **17**:175-199.
- Ernst W.G., Liu J. 1998. Experimental phase-equilibrium study of Al- and Ti-contents of calcic amphibole in MORB—A semiquantitative thermobarometer. *American Mineralogist*, **83**(9-10):952-969. <https://doi.org/10.2138/am-1998-9-1004>
- Ferreira J.A.M., Albuquerque J.P.T. 1969. *Sinopse da geologia da Folha Seridó*. Recife, SUDENE, DRN/DG, Série Geológica, 52 p. (Boletim 18).
- Ferreira V.P., Sial A.N., Jardim de Sá E.F. 1998. Geochemical and isotopic signatures of Proterozoic granitoids in terrenes of the Borborema structural province, northeastern Brazil. *Journal of South America Earth Sciences*, **11**(5):439-455. [https://doi.org/10.1016/S0895-9811\(98\)00027-3](https://doi.org/10.1016/S0895-9811(98)00027-3)
- Finger F., Schiller D. 2012. Lead contents of S-type granites and their petrogenetic significance. *Contributions to Mineralogy and Petrology*, **164**(5):747-755. <https://doi.org/10.1007/s00410-012-0771-3>
- France L., Ildefonso B., Koepke J., Bech F. 2010. New method to estimate the oxidation state of basaltic series from microprobe analyses. *Journal of Volcanology and Geothermal Research*, **189**(3-4):340-346. <https://doi.org/10.1016/j.jvolgeores.2009.11.023>
- Frost B.R., Barnes C.G., Collins W.J., Arculus R.J., Ellis D.J., Frost C.D. 2001. A geochemical classification of granitic rocks. *Journal of Petrology*, **42**(11):2033-2048. <https://doi.org/10.1093/petrology/42.11.2033>
- Gill J.B. 1981. *Orogenic Andesites and Plate Tectonics*. Berlin, Heidelberg, New York: Springer-Verlag, 390 p.
- Guimaraes I.P., Brito M.F.L., Lages G.A., Silva Filho A.F., Santos L., Brasilino R.G. 2016. Tonian granitic magmatism of the Borborema Province, NE Brazil: A review. *Journal of South American Earth Science*, **68**:97-112. <https://doi.org/10.1016/j.jsames.2015.10.009>
- Guimaraes I.P., Da Silva Filho A.F. 1998. Nd- and Sr isotopic and U-Pb geochronologic constraints for the evolution of the shoshonitic Brasiliano Bom Jardim and Toritama complexes: evidence for a Transamazonian enriched mantle under Borborema tectonic province, Brazil. *International Geology Review*, **40**(6):500-527. <https://doi.org/10.1080/00206819809465221>
- Guimaraes I.P., Da Silva Filho A.F., de Araújo D.B., de Almeida C.N., Dantas E. 2009. Trans-alkaline magmatism in the Serrinha-Pedro Velho Complex, Borborema Province, NE Brazil and its correlations with the magmatism in eastern Nigeria. *Gondwana Research*, **15**(1):98-110. <https://doi.org/10.1016/j.gr.2008.06.011>

- Guimarães I.P., Silva Filho A.F., Almeida C.N., Van Schmus W.R., Araújo J.M.M., Melo S.C., Melo E.B. 2004. Brasiliano (Pan-African) granitic magmatism in the Pajeú -Paraíba belt, Northeast Brazil: an isotopic and geochronological approach. *Precambrian Research*, **135**:23-53.
- Hammarstrom J.M., Zen E. 1986. Aluminum in hornblende: an empirical igneous geobarometer. *American Mineralogist*, **71**(11-12):1297-1313.
- Hofmeister A.M., Rossman G.R. 1985. A spectroscopic study of irradiation coloring of amazonite: structurally hydrous, Pb-bearing feldspar. *American Mineralogist*, **70**(7-8):794-804.
- Hollanda M.H.B.M., Archanjo C.J., Souza L.C., Dunyi L., Armstrong R. 2011. Longlived Paleoproterozoic granitic magmatism in the Seridó-Jaguaribe domain, Borborema Province-NE Brazil. *Journal of South American Earth Sciences*, **32**(4):287-300. <http://dx.doi.org/10.1016/j.jsames.2011.02.008>
- Hollanda M.H.B.M., Pimentel M.M., Jardim de Sá E.F. 2003. Paleoproterozoic subductionrelated metasomatic signatures in the lithospheric mantle beneath NE Brazil: inferences from trace element and Sr-Nd-Pb isotopic compositions of Neoproterozoic high-K igneous rocks. *Journal of South American Earth Sciences*, **15**(8):885-900. [https://dx.doi.org/10.1016/S0895-9811\(03\)00014-2](https://dx.doi.org/10.1016/S0895-9811(03)00014-2)
- Hollister L.S., Grissom G.C., Peters E.K., Stowell H.H., Sisson V.B. 1987. Confirmation of the empirical correlation of Al-in-hornblende with pressure of solidification of calc-alkaline plutons. *American Mineralogist*, **72**(3-4):231-239.
- Ishihara S. 1998. Granitoid series and mineralization in the Circum-Pacific Phanerozoic granitic belts: *Resource Geology*, **48**(4):219-224. <https://dx.doi.org/10.1111/j.1751-3928.1998.tb00019.x>
- Jackson S.E., Pearson N.J., Griffin W.L., Belousova E.A. 2004. The application of laser ablation-inductively coupled plasma-mass spectrometry to in situ U-Pb zircon geochronology. *Chemical Geology*, **211**(1-2):47-69. <https://doi.org/10.1016/j.chemgeo.2004.06.017>
- Jardim de Sá E.F. 1994. *A Faixa Seridó (Província Borborema, NE do Brasil) e o seu significado geodinâmico na Cadeia Brasileira/Pan-Africana*. Thesis, Instituto de Geociências, Universidade de Brasília, Brasília, 804 p.
- Jardim de Sá E.F., Legrand J.M., McReath I. 1981. "Estratigrafia" de rochas granitoides na região do Seridó (RN-PB) com base em critérios estruturais. *Revista Brasileira de Geociências*, **11**(1):50-57.
- Johnson M.C., Rutherford M.J. 1988. Experimental calibration of an Aluminum-in-hornblende geobarometer applicable to calc-alkaline rocks. *EOS*, **69**:1511.
- Johnson M.C., Rutherford M.J. 1989. Experimental calibration of the aluminum-in-hornblende geobarometer with application to Long Valley caldera (California) volcanic rocks. *Geology*, **17**(9):837-841. [https://doi.org/10.1130/0091-7613\(1989\)017%3C0837:ECOTAI%3E2.3.CO;2](https://doi.org/10.1130/0091-7613(1989)017%3C0837:ECOTAI%3E2.3.CO;2)
- Leake B.E., Woolley A.R., Arps C.E.S., Birch W.D., Gilbert M.C., Grice J.D., Hawthorne F.C., Kato A., Kisch H.J., Krivovichev V.G., Linthout K., Laird J., Mandarino J., Maresch W.V., Nickel E.H., Rock N.M.S., Schumacher J.C., Smith D.C., Stephenson N.C.N., Ungaretti L., Whittaker E.J.W., Youzhi G. 1997. Nomenclature of amphiboles: Report of the subcommittee on amphiboles of the International Mineralogical Association Commission on New Minerals and Mineral Names. *Canadian Mineralogist*, **35**(1):219-246.
- Leterrier J., Jardim de Sá E.F., Bertrand J.M., Pin C. 1994. Ages U-Pb sur zircon de granitoides "brasiliens" de la ceinture do Seridó (Province Borborema, NE Brésil). *Comptes Rendus Mathématique Academie des Sciences*, **318**:1505-1511.
- Loiselle M.C., Wones D.R. 1979. Characteristics of Anorogenic Granites. *Geological Society of America, Abstracts with Programs*, **11**:468.
- London D. 2008. *Pegmatites*. Canada, The Canadian Mineralogist Special Edition, 368 p.
- Mader U.K., Berman R.G. 1992. Amphibole thermobarometry, a thermodynamic approach, Current Research - Part E. *Geological Survey of Canada Paper*, **92**(1E):393-400. <https://doi.org/10.4095/133594>
- Martin R. 2004. Where do LCT and NYF pegmatites fit in? A contribution to a revised classification of granitic pegmatites. *Geological Society of America Denver Annual Meeting Abstracts with Programs*, **36**(5):44.
- Martin R.F., De Vito C., Pezzotta F. 2008. Why is amazonite K-feldspar an earmark of NYF-type granitic pegmatites: clues from hybrid pegmatites in Madagascar. *American Mineralogist*, **93**(2-3):263-269. <https://doi.org/10.2138/am.2008.2595>
- McKeough M.A., Lentz D.R., McFarlane C.R.M., Brown J. 2013. Geology and evolution of pegmatite-hosted U-Th ± REE-Y-Nb Mineralization, Kulyk, Eagle, and Karin Lakes region, Wollaston Domain, northern Saskatchewan, Canada: examples of the dual role of extreme fractionation and hybridization processes. *Journal of Geosciences*, **58**:321-346. <https://doi.org/10.3190/jgeosci.153>
- McMurry J., Long L.E., Sial A.N. 1987. Petrology and isotope systematics of magma mushes: some porphyritic granitoids of northeastern Brazil. *Revista Brasileira de Geociências*, **17**(4):473-480.
- Medeiros V.C., Amaral C.A., Rocha D.E.G.A. 2005. *Programa de Geologia do Brasil – PGB*. Folha SB.24-Z-A Sousa. Escala 1:250.000. Recife, CPRM.
- Meunier A.R. 1964. Succession stratigraphique et passages lateraux dus au metamorphisme dans la Série Ceará, Antecambrien du Nord-Est brésilien. *Comptes Rendus Mathématique Academie des Sciences*, **259**:3796-3799.
- Nachit H., Razafimahefa N., Stussi J.M., Carron J.P. 1985. Composition chimique des biotites et typologie magmatique des granitoides. *Comptes Rendus Mathématique Academie des Sciences*, **301**: 813-818.
- Nakamura N. 1974. Determination of REE, Ba, Mg, Na and K in carbonaceous and ordinary chondrites. *Geochimica et Cosmochimica Acta*, **38**(5):757-775. [https://doi.org/10.1016/0016-7037\(74\)90149-5](https://doi.org/10.1016/0016-7037(74)90149-5)
- Nascimento M.A.L., Antunes A.F., Galindo A.C., Jardim de Sá E.F., Souza Z.S. 2000. Geochemical signatures of the Brasiliano-age plutonism in the Seridó belt, Northeastern Borborema Province (NE Brazil). *Revista Brasileira de Geociências*, **30**(1):161-164.
- Nascimento M.A.L., Galindo A.C., Medeiros V.C. 2015. Ediacaran to Cambrian magmatic suites in the Rio Grande do Norte domain, extreme Northeastern Borborema Province (NE of Brazil): Current knowledge. *Journal of South American Earth Sciences*, **58**:281-299. <https://doi.org/10.1016/j.jsames.2014.09.008>
- Neves S.P., Bruguier O., Bosh D., Silva J.M.R., Mariano G. 2008. U-Pb ages of plutonic and metaplutonic rocks in southern Borborema Province (NE Brazil): timing of Brasiliano deformation and magmatism. *Journal of South American Earth Sciences*, **25**:285-297. <https://doi.org/10.1016/j.jsames.2007.06.003>
- Neves S.P., Bruguier O., Vauchez A., Bosch D., Silva J.M.R., Mariano G. 2006. Timing of crust formation, deposition of supracrustal sequences, and Transamazonian and Brasiliano metamorphism in the East Pernambuco belt (Borborema Province, NE Brazil): Implications for western Gondwana assembly. *Precambrian Research*, **149**(3-4):197-216. <https://doi.org/10.1016/j.precamres.2006.06.005>
- Neves S.P., Mariano G. 1999. Assessing the tectonic significance of a large-scale transcurrent shear zone system: The Pernambuco lineament, northeastern Brazil. *Journal of Structural Geology*, **21**(10):1369-1383. [https://doi.org/10.1016/S0191-8141\(99\)00097-8](https://doi.org/10.1016/S0191-8141(99)00097-8)
- Neves S.P., Vauchez A., Feraud G. 2000. Tectono-thermal evolution, magma emplacement, and shear zone development in the Caruaru area (Borborema Province, NE Brazil). *Precambrian Research*, **99**(1-2):1-32. [https://doi.org/10.1016/S0301-9268\(99\)00026-1](https://doi.org/10.1016/S0301-9268(99)00026-1)
- Ostrooumov M., Banerjee A. 2005. Typomorphic features of amazonitic K-feldspar from the Keivy granitic pegmatite (Kola Peninsula, Russia). *Schweizerische Mineralogische und Petrographische Mitteilungen*, **85**(1):89-102.
- Pearce J.A. 1996. A User's Guide to Basalt Discrimination Diagrams. In: Wyman D.A. (ed.), *Trace Element Geochemistry of Volcanic Rocks: Applications for Massive Sulphide Exploration*. Geological Association of Canada, Short Course Notes, v. 12, p. 79-113.
- Pearce J.A., Bender J.F., De Long S.E., Kidd W.S.F., Low P.J., Güner Y., Saroglu F., Yilmaz Y., Moorbath S., Mitchell J.G. 1990. Genesis of collision volcanism in Eastern Anatolia, Turkey. *Journal of Volcanology and Geothermal Research*, **44**(1-2):189-229.
- Pearce J.A., Harris N.B.W., Tindle A.G. 1984. Trace element discrimination diagrams for the tectonic interpretation of granitic rocks. *Journal of Petrology*, **25**(4):956-983. <https://doi.org/10.1093/petrology/25.4.956>
- Rogers J.W. 1996. A History of Continents in the Past Three Billions Years. *The Journal of Geology*, **104**(1):91-107.

- Rutter M.J., Van der Laan S.R., Wyllie P.J. 1989. Experimental data for a proposed empirical igneous geobarometer: Aluminium in hornblende at 10 kbar pressure. *Geology*, **17**(10):897-900. [https://doi.org/10.1130/0091-7613\(1989\)017%3C0897:EDFAPE%3E2.3.CO;2](https://doi.org/10.1130/0091-7613(1989)017%3C0897:EDFAPE%3E2.3.CO;2)
- Sá J.M., Sousa L.C., Legrand J.M., Galindo A.C., Maia H.N., Fillippi R.R. 2014. U-Pb and Sm-Nd data of the Rhyacian and Statherian Orthogneisses from Rio Piranhas-Seridó and Jaguaribeano Terranes, Borborema Province, Northeast of Brazil. *Revista do Instituto de Geociências, Série Científica*, **14**(3):97-110. <https://doi.org/10.5327/Z1519-874X201400030007>
- Santos E.J., Souza Neto J.A., Silva M.R.R., Beurlen H., Cavalcanti J.A.D., Silva M.G., Costa A.F., Santos L.C.M.L., Santos R.B. 2014. Metalogênese das porções norte e central da Província Borborema. In: Silva M.G., Neto M.B.R., Jost H., Kuyumjian R.M. (eds.), *Metalogênese das Províncias Tectônicas Brasileiras*. Brasil, CPRM, p. 343-388.
- Schmidt M.W. 1992. Amphibole composition in tonalite as a function of pressure: An experimental calibration of the Al-in-hornblende barometer. *Contributions to Mineralogy and Petrology*, **110**:304-310. <https://doi.org/10.1007/BF00310745>
- Silva J.M.R., Mariano G. 2000. Geometry and kinematics of the Afogados da Ingazeira shear zone, northeast Brazil. *International Geology Review*, **42**(1):86-95. <https://doi.org/10.1080/00206810009465071>
- Silva Filho A.F., Guimarães I.P., Santos L., Armstrong R., Van Schmus W.R. 2016. Geochemistry, U-Pb geochronology, Sm-Nd and O isotopes of ca. 50 Ma long Ediacaran High-K Syn-Collisional Magmatism in the Pernambuco Alagoas Domain, Borborema Province, NE Brazil. *Journal of South American Earth Sciences*, **68**:134-154. <https://doi.org/10.1016/j.jsames.2015.12.013>
- Snook B. 2014. *Towards exploration tools for high purity quartz: An example from the South Norwegian Ejeveland pegmatite belt*. Thesis, Camborne School of Mines, University of Exeter.
- Souza J.V. 1985. *Geologia dos pegmatitos de metais raros da região W e NW de Solonópole - CE*. Fortaleza. Tese, Departamento de Geologia, Universidade Federal do Ceará, Fortaleza, 109 p.
- Souza Z.S., Martin H., Peucat J.J., Jardim de Sá E.F., Macedo M.H.F. 2007. Calc-alkaline magmatism at the archaic-proterozoic transition: the Caicó Complex basement (NE Brasil). *Journal of Petrology*, **48**(11):2149-2185. <https://doi.org/10.1093/petrology/egm055>
- Spear F.S. 1981. An experimental study of hornblende stability and compositional variability in amphibolite. *American Journal of Science*, **281**:697-734. <https://doi.org/10.2475/ajs.281.6.697>
- Sun S.S. 1980. Lead isotopic study of young volcanic rocks from mid-ocean ridges, oceanic islands and island arcs. *Philosophical Transactions of the Royal Society of London*, **A297**(1431):409-445. <https://doi.org/10.1098/rsta.1980.0224>
- Trindade R.I., Dantas E.L., Babinski M., Schmus W.R.V. 1999. Shortlived granitic magmatism along shear zone: evidence from U-Pb zircon and sphene age of Caraúbas and Tourão granite. In: South American Symposium on Isotope Geology, 2, Argentina. *Actas*, p. 143-144.
- Tulloch A.J., Challis G.A. 2000. Emplacement depths of Paleozoic-Mesozoic plutons from western New Zealand estimated by hornblende-Al geobarometry. *New Zealand Journal of Geology and Geophysics*, **43**(4):555-567. <https://doi.org/10.1080/00288306.2000.9514908>
- Van Schmus W.R., Brito Neves B.B., Hackspacher P., Babinski M. 1995. U/Pb and Sm/Nd geochronologic studies of eastern Borborema Province, northeastern Brazil: initial conclusions. *Journal of South American Earth Sciences*, **8**(3-4):267-288. [https://doi.org/10.1016/0895-9811\(95\)00013-6](https://doi.org/10.1016/0895-9811(95)00013-6)
- Van Schmus W.R., Kozuch M., Brito Neves B.B. 2011. Precambrian history of the Zona Transversal of the Borborema Province, NE Brazil; Insights from Sm-Nd and U-Pb geochronology. *Journal of South American Earth Sciences*, **31**(2-3):227-25. <https://dx.doi.org/10.1016/j.jsames.2011.02.010>
- Van Schmus W.R., Oliveira E.P., Silva Filho A.F., Toteu S.F., Penaye J., Guimarães I.P. 2008. Proterozoic links between the Borborema Province, NE Brazil, and the Central African Fold Belt. *Geological Society of London, Special Publication*, **294**:69-99. <https://doi.org/10.1144/SP294.5>
- Vauchez A., Egydio-Silva M. 1992. Termination of a continental scale strike-slip fault in partially melted crust: The West-Pemambuco shear zone, northeast Brazil. *Geology*, **20**(11):1007-1010. [https://doi.org/10.1130/0091-7613\(1992\)020%3C1007:TOACSS%3E2.3.CO;2](https://doi.org/10.1130/0091-7613(1992)020%3C1007:TOACSS%3E2.3.CO;2)
- Vidal F.W.H., Nogueira Neto J.A. 2005. Minerais de Pegmatitos. In: Vidal F.W.H., Sales F.A.C.B., Roberto F.A.C., Sousa J.F., Mattos I.C. *Rochas e Minerais Industriais do Estado do Ceará*. Fortaleza, CETEM / UECE / DNPMP / FUNCAP / SENAI, p. 67-82.
- Watson E.B. 1979. Zircon saturation in felsic liquids: experimental results and applications to trace element geochemistry. *Contributions to Mineralogy and Petrology*, **70**(4):407-419. <https://doi.org/10.1007/BF00371047>
- Watson E.B., Harrison T.M. 1983. Zircon saturation revisited: temperature and composition effects in a variety of crustal magma types. *Earth Planet Science Letters*, **64**(2):295-304. [https://doi.org/10.1016/0012-821X\(83\)90211-X](https://doi.org/10.1016/0012-821X(83)90211-X)
- Watson E.B., Harrison T.M. 1984. Accessory phases and the geochemical evolution of crustal magmas. *Physics of the Earth and Planetary Interiors*, **35**(1-3):19-30. [https://doi.org/10.1016/0031-9201\(84\)90031-1](https://doi.org/10.1016/0031-9201(84)90031-1)
- Williams C.T. 1996. Analysis of rare earth minerals. In: Jones A., Wall F., Williams C.T. (eds.), *Rare Earth Minerals: Chemistry Origin and Ore Deposits*. London, Chapman and Hall, p. 193-226.
- Williams I.S., Claesson S. 1987. Isotopic evidence for the Precambrian provenance and Caledonian metamorphism of high grade paragneisses from the Seven Nappes, Scandinavian Caledonides. Ion microprobe zircon U-Pb-Th. *Contribution to Mineralogy and Petrology*, **97**(2):205-217. <https://doi.org/10.1007/BF00371240>
- Wise M.A. 1999. Characterization and classification of NYF-type pegmatites. *Canadian Mineralogist*, **37**(Part 3):802-803.
- Wise M.A. 2017. Mineralogy and mineral chemistry of NYF-type granitic pegmatites. *NGF Abstracts and Proceedings*, **2**:177-180.
- Wones D.R. 1989. Significance of the assemblage titanite + magnetite + quartz in granitic rocks. *American Mineralogist*, **74**(7-8):744-749.